FRONTIERS OF PHYSICS

TOPICAL REVIEW
Volume 19 / Issue 2 / 23502 / 2024

Quasi-two dimensional Ruddlesden–Popper halide perovskites for laser applications

Kun Chen[1,2,*], Qianpeng Zhang[1,2,*], Yin Liang[2,*], Jiepeng Song[2], Chun Li[2], Shi Chen[3], Fang Li[1,†], Qing Zhang[2,‡]

1 School of Mechanical and Electrical Engineering, Wuhan Institute of Technology, Wuhan 430205, China
2 School of Materials Science and Engineering, Peking University, Beijing 100871, China
3 Institute of Applied Physics and Materials Engineering, Macau University, Macao 999078, China
*These three authors contributed equally to this work.
Corresponding authors. E-mail: †Lifang@wit.edu.cn, ‡Q_zhang@pku.edu.cn
Received April 10, 2023; accepted May 26, 2023

ABSTRACT

Quasi-two-dimensional (2D) Ruddlesden–Popper (RP) halide perovskites, as a kind of emerged two-dimensional layered materials, have recently achieved great attentions in lasing materials field owing to their large exciton binding energy, high emission yield, large optical gain, and wide-range tuning of optical bandgap. This review will introduce research progresses of RP halide perovskites for lasing applications in aspects of materials, photophysics, and devices with emphasis on emission and lasing properties tailored by the molecular composition and interface. The materials, structures and fabrications are introduced in the first part. Next, the optical transitions and amplified spontaneous emission properties are discussed from the aspects of electronic structure, exciton, gain dynamics, and interface tailoring. Then, the research progresses on lasing devices are summarized and several types of lasers including VCSEL, DFB lasers, microlasers, random lasers, plasmonic lasers, and polariton lasers are discussed. At last, the challenges and perspectives would be provided.

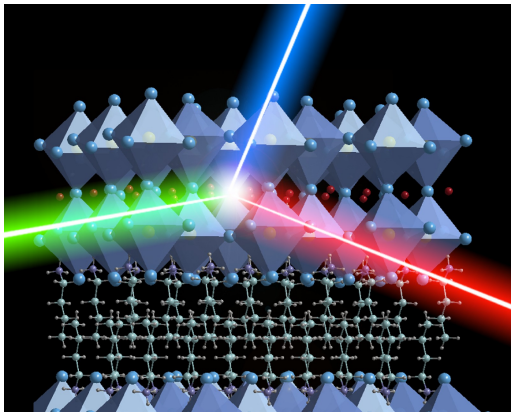

Keywords two-dimensional materials, metal halide perovskite, Ruddlesden–Popper halide perovskites, lasing, emission

Contents

*Special Topic: Surface and Interface of Two-dimensional Materials (Eds.: Lijun Zhang, Dongchen Qi, Ming Yang & Kai Zhang).

Higher Education Press

https://doi.org/10.1007/s11467-023-1347-6

1 Introduction

In recent years, quasi-two-dimensional (2D) Ruddlesden–Popper (RP) perovskites have attracted wide attention in scientific and application fields [1, 2]. The excellent optical and electrical properties of RP perovskites, such as high photoluminescence (PL) quantum efficiency with high radiative recombination rate and tunable emission wavelength as well as low cost and scalability, make them one of the materials with the potential to achieve high-efficiency and low-cost optoelectronic devices, including solar cells, photodetectors, lasers and photocatalysts [3–9]. Compared with 3D perovskites, the RP perovskites have a faster charge transfer rate and higher stability [10–12]. Moreover, the emission properties of RP perovskites can be easily tuned by controlling the composition, dimension and interface. Therefore, RP perovskites can be used as gain media to achieve wavelength-tunable, high-output-power and low-cost lasers. In recent years, numerous successes have been achieved in the fabrication of RP perovskite-based lasers and the realization of high-efficiency laser outputs at different wavelengths.

This review aims to summarize the research progresses of RP perovskites in laser applications. In Section 2, we introduce the crystal structures, materials, and fabrications of RP perovskites. In Section 3, we introduce the electronic structure of RP perovskites, the relationship between excitons and emission characteristics as well as the tuning of emission characteristics. In Section 4, we discuss the amplified spontaneous emission of RP perovskites. In Section 5, we summarize the progresses of photonic lasers based on RP perovskites. In Section 6, we discuss the exciton–photon interaction and exciton–polariton condensation of RP perovskites, as well as their application prospects in the laser field. Finally, we provide some perspectives on the RP perovskite laser studies and applications. Through this review, we aim to provide a comprehensive and systematic framework of research progress on RP perovskite laser applications for relevant researchers and to provide new ideas and inspirations for RP perovskite laser applications, promoting their applications in relevant fields.

2 Materials and fabrications of RP perovskites

2.1 Materials

RP perovskites have a structural formula of $R_2A_{n-1}B_nX_{3n+1}$, where R usually represents a long-chained organic ammonium cation, such as BA (butylamine) or PEA (phenethylamine); A is generally a small monovalent cation, such as Cs, FA (formamidinium), or MA (methylammonium); B is generally a large transition metal cation, such as Pb or Sn; X is generally a halogen anion, such as Cl, Br, or I; and n is the number of inorganic layers. The quasi-2D structure is constructed by "cutting" 3D perovskite crystals with large organic cations, where octahedral $[BX_6]^{4-}$ forms inorganic layers, organic cations form organic layers and inorganic as well as organic layers stack each other to form a sandwich like structure. When there is only one $[BX_6]^{4-}$ inorganic layer between two large organic ligands, i.e., n=1, it is called 2D perovskite. When there are multiple interconnected $[BX_6]^{4-}$ inorganic layers between two organic layers, i.e., n>1 but limited, it is called quasi-2D perovskite. When n is infinite, the octahedral $[BX_6]^{4-}$ forms a network structure with small A-site cations distributed among them, forming a 3D perovskite ABX_3.

The layered structure of RP perovskites gives rise to many physical properties. On the one hand, the layered structure provides effective channels for carrier transport, resulting in higher carrier mobility and lifetime [13]. On the other hand, the presence of van der Waals gaps amongst organic ligands facilitates the process of delamination of the layered structure. Compared to 3D perovskites, RP perovskites show increased resilience towards larger and more intricate organic ligands, thereby enhancing the adaptability and customization of their structures [14]. Moreover, the RP perovskites' composition of multiple quantum wells endows them with heightened exciton binding energy and adjustable quantum confinement effects [15].

2.2 Fabrications

Solution-processed thin films, single crystals, and quantum dots have been fabricated for the RP halide perovskites. Compared to 3D perovskites, the RP halide perovskite films are easier to manufacture into large area, controllable thickness films, which are compatible with the manufacturing processes of thin film solar cells and light emitting diodes (LEDs) [16, 17]. For example, the highest external quantum efficiency (EQE) achieved for RP perovskite LEDs is 28.1% using $PEA_2Cs_4Pb_5Br_{16}$, and the best photon conversion efficiency (PCE) of 18.24% for RP

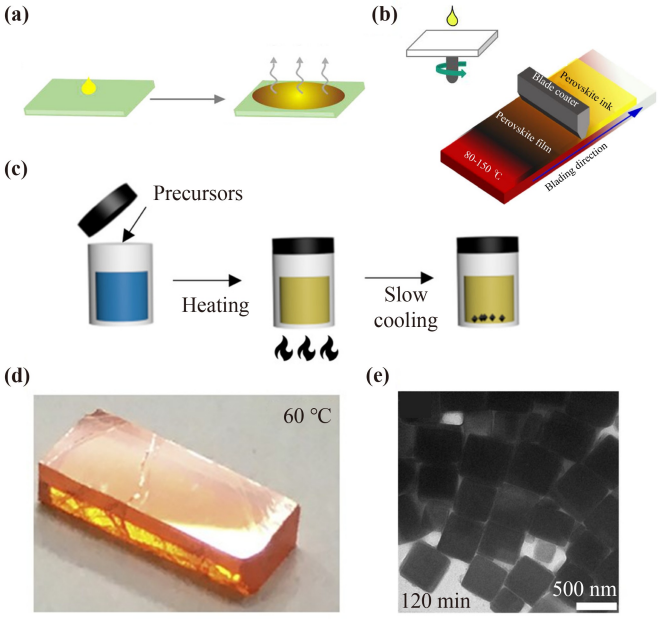

Fig. 1 Materials and fabrications of RP perovskite. **(a)** Drop casting preparation method. **(b)** Spin coating and Blade coating preparation method. **(c)** Slow cooling preparation method. **(d)** $(PEA)_2PbI_4$ crystals taken at 60 ℃. **(e)** Superlattice nanocrystals. (a) Reproduced from Ref. [20]. (b) Reproduced from Refs. [21, 22]. (c) Reproduced from Ref. [25]. (d) Reproduced from Ref. [26]. (e) Reproduced from Ref. [31].

perovskite solar cells was achieved through heat-light co-treatment using $GA_{0.2}BA_{1.8}MA_5Pb_6I_{19}$ [5, 18]. Moreover, the RP perovskite polycrystalline films naturally contain mixed phases to construct cascade energy or carrier transfer systems that significantly enhance the radiation recombination efficiency compared to pure-phased films [1].

The process of producing RP halide perovskite films generally involves spin coating and the following annealing treatment. To avoid the large temperature change detrimental to the film crystallinity, non-spin-coated methods, including drop-casting, batch slot-die coating, and roll-to-roll slot-die coating method were utilized to fabricate RP halide perovskite films [Figs. 1(a, b)], which are simple and easy to scale up [19–22]. Compared to these polycrystalline thin films, the single crystal materials have a low defect and impurity density [23]. Currently, several techniques have been devised for the growth of RP perovskite single crystals, such as the anti-solvent diffusion method and the slow cooling method [Fig. 1(c)] [24, 25]. For example, to grow large-scale RP perovskites, a surface-tension-assisted crystallization was proposed to control the orientation of small single crystallite, realizing the fabrication of $(PEA)_2PbI_4$ single crystals with 36 mm in length [Fig. 1(d)] [26].

Quantum dots are considered as favorable options for display technology in low-dimensional systems because they exhibit a substantial luminescence quantum yield [27]. Recently, the perovskite quantum dots have been receiving much attention [28]. Although a large number of organic ligands are introduced to maintain their stability in solvents, the cooling or solvent evaporation in crystallization method hinders the fine engineering of quantum dots on the nanoscale [29, 30]. To address this problem, a layer-by-layer self-assembly method was developed, providing a general approach for the atomic precision engineering of 2D RP perovskites as well as synthesizing other 2D layered superlattice nanomaterials [Fig. 1(e)] [31].

Moreover, the synthesis routes have significant effects on the morphology, crystal quality, and characteristics of perovskites. For instance, to reduce the trap state density and energy disorder in polycrystalline films, a brominated aromatic amine trimer is designed as an antisolvent dissolving in the perovskite precursors, which accessed the grain boundary and mitigated the defects [32]. Nevertheless, the solution processing involves complex crystal growth factors. In comparison, the vapor deposition method has more advantages, with chemical gases or vapors reacting on a substrate surface. Recently, by combining solution synthesis and chemical vapor deposition, both lateral and vertical RP perovskite heterostructures were successfully synthesized utilizing a shadow mask to tune the growth orientations [33].

2.3 Dimension, organic–inorganic interface and molecular tuning

By altering the dimension, organic-inorganic interface and molecular structure, RP perovskites can exhibit improved stability and superior properties over other perovskites. First, the quantum and dielectric confinement can be effectively tuned by engineering the inorganic part thickness, rendering tunable bandgap and exciton binding energy [34]. Moreover, it is reported that the Auger recombination rate and electron–phonon coupling strength decrease with increasing inorganic part thickness due to suppressed overlap of carrier wavefunctions and increased lattice rigidity, respectively, which lowers the lasing threshold [35]. Besides, modifying the precursor molecules and pH value of the solution can control the morphology and dimension of RP perovskite, which not only facilitates carrier transport and prevents charge accumulation, but also tunes the emission from green to blue [4].

Altering the organic–inorganic interface can also effectively adjust the optical and electronic properties of the RP perovskite materials. For example, by applying hydrostatic pressure, the band alignment at the inorganic –organic interface can be reconfigured, and pressure-gated on-off emission states have been achieved [36]. Further, tuning the spacer cations can enable the preferable vertical crystal orientation and optimize the efficiency of optoelectronics devices. Meanwhile, by adjusting the

dipole moments of organic cations, such as PEA^+ and *p*-$FPEA^+$, the Auger recombination is suppressed and the bandgap energy is decreased [37–39]. Besides, the FuMA ligand with an aromatic furan ring shortened the distance between inorganic layers, enhancing the structural durability and water resilience of the thin film [40].

3 Emission properties of RP halide perovskites

3.1 Electronic structures

The electronic structure of RP perovskites forms the basis of their emission performance, with the most important electronic structures being the valence band and the conduction band. Taking lead iodide-based RP perovskites as an example, the Pb-I octahedron has a significant contribution to their electronic structure (similar to 3D perovskites) [41]: the Pb-*s* and I-*p* antibonding molecular orbital form the top of the valence band and the Pb-*p* orbital forms the bottom of the conduction band. The A-site cations, whether inorganic or organic cations, mainly ensure the structural integrity, with limited impact on charge transport behavior [42]. Nevertheless, the electronic structures of RP perovskites differ from those of 3D perovskites. Firstly, the bandgap of RP perovskites is larger than that of 3D perovskites because in quasi-2D structures, electrons are strongly confined in the dimension perpendicular to the transport direction, which restricts electronic transitions between the valence and conduction bands in the absorption process [43]. This confinement can result in strong quantum confinement effect, leading to highly anisotropic electronic properties [44]. Secondly, the electronic structure of RP perovskites exhibits stronger spin polarization effects. This effect can cause many interesting phenomena, such as spin-polarization-induced ferroelectricity, magnetoelectric effects and spin Hall effects, which will change the electrical and magnetic properties of RP perovskites [45].

3.2 Excitons

Excitons are bound states formed by the strong interaction between electrons and holes and their energy is much lower than that of individual electrons or holes. Excitons play an important role in RP perovskites because they can absorb photons and convert them into excitonic excited states, leading to the luminescent and emissive properties of the material. Excitons can also interact with each other to form exciton–exciton and exciton-charge carrier complexes, thereby affecting the optical and electrical properties. Additionally, due to the soft lattice of RP perovskites, free excitons could be trapped by octahedral distortion through strong electron phonon interactions, forming the self-trapped excitons. Self-trapped excitons exhibit a broadband emission and a large Stokes shift (> 100 meV), holding great potentials for display and narrowband detection [46, 47].

Excitons in RP perovskites are influenced by geometric restrictions and interface effects. The quantum well and dielectric constant of RP perovskites are directly related to the *n*-value, which affects the exciton binding energy. For example, when *n* decreases from 5 to 1, the exciton binding energy of $(BA)_2(MA)_{n-1}Pb_nI_{3n+1}$ crystal increases from 220 meV to 380 meV [48]. Compared with 3D perovskites, RP perovskites have thin and deep quantum wells, which reduces the Bohr radius and increases the exciton binding energy [13], making it possible to observe RP perovskite excitons at room temperature. Further, the large exciton binding energy in RP halide perovskites can produce important physical phenomena in RP halide perovskites, such as exciton–polariton [49]. This exciton–polariton has an exceptionally strong nonlinear optical response, which will be discussed in detail in Section 6.

3.3 Emission dynamics and properties

The emission characteristics of RP perovskites are closely related to the crystal structure, chemical composition, and surface properties, through which the emission properties of RP perovskites can be modulated.

First, metal ion doping can alter the band structure of RP perovskites, resulting in changes in the emission wavelength. Recent studies have successfully achieved stable yellow LED by doping Rb^+ into $(BA)_2CsPb_2I_7$ perovskite [50]. As shown in Fig. 2(a), the doping of Rb^+ led to the tilting of PbI_6 octahedra, caused a red shift of the emission peak and ultimately achieved a stable emission peak at 595 nm. Metal ion doping can also form an alloy structure of RP perovskites. For example, by introducing both Rb^+ and Cl^- ions into PEA-$CsPbBr_3$, Cl^- alloying can result in blue shift of emission, while Rb^+ alloying can promote the formation of 2D phase components, thereby forming sub-micron-sized particles on the surface of the film, and improving the light output coupling efficiency [51]. In addition, metal ion doping at an appropriate concentration can fill the defect sites of RP perovskites. As shown in Fig. 2(b), Mn^{2+} doping improved the surface morphology of RP perovskite thin films, changed the emission wavelength and simultaneously lowered the trap density, thereby enhancing the energy transfer efficiency [52].

The chemical composition of RP perovskites can affect their band structure and emission characteristics, with varying the proportion of organic cations being a common method. As shown in Fig. 2(c), the schematic diagram of the layered structure of $(PEA)_2PbI_4$, $(NMA)_2PbI_4$ and $(PEA)(NMA)PbI_4$ reveals the influence of different chemical compositions on the RP perovskite structure [53]. By controlling the molar ratio of PEA

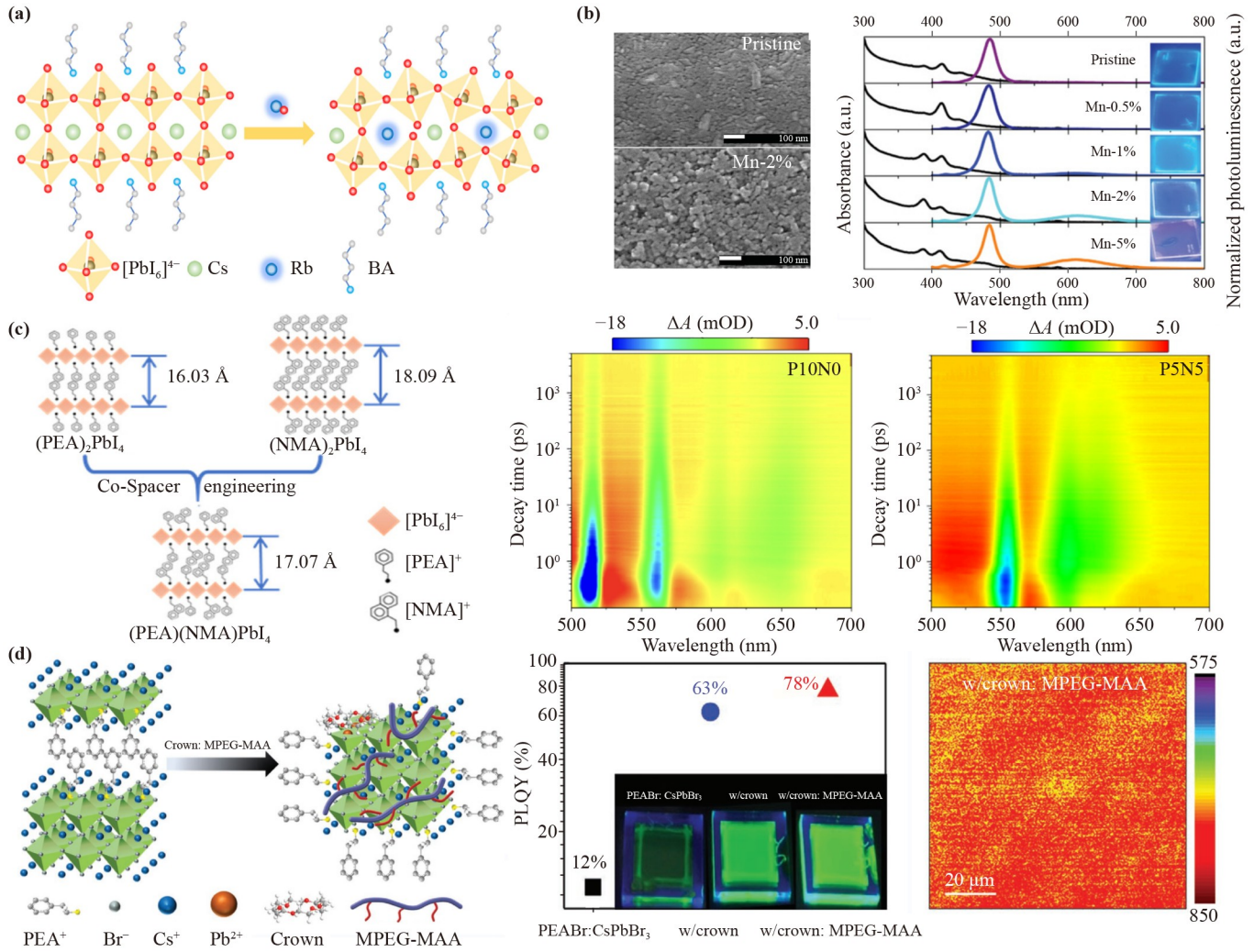

Fig. 2 Emission property regulation of RP perovskite. **(a)** Schematic diagram of the effect of doping Rb^+ on PbI_6 octahedra. **(b)** The left figure shows the SEM image of undoped and Mn-2% doped sample and the right figure shows the PL and UV-vis absorption diagram of the sample doped with different concentrations of Mn. **(c)** The left image shows schematic diagrams of the layered structures of PEA, NMA and mixed PEA, NMA perovskites, while the right image displays a colored plot of the TA spectra of perovskite films with varying ratios of PEA and NMA cations. **(d)** The left figure shows the schematic diagram of crown ether and MPEG-MAA changing the crystal structure and passivating defects, the middle figure shows the PL quantum yield of different perovskite films, and the right figure shows the confocal PL intensity diagram of perovskite films with MPEG-MAA. (a) Reproduced from Ref. [50]. (b) Reproduced from Ref. [52]. (c) Reproduced from Ref. [53]. (d) Reproduced from Ref. [5].

and NMA, the phase distribution of the material can be effectively adjusted to achieve emission of different colors. Among them, the LEDs with a molar ratio of 5:5 of PEA and NMA exhibit high-purity red electroluminescence. In addition, recent studies have achieved high-quality PBAI-$CsPbBr_xI_{3-x}$-PEOXA composite films by adjusting the molar ratio of cations and anions, with emission adjustable in the range of pure red to deep red [54]. The use of different organic cations is also an effective method. Organic cations with different dipole moments can tune the band edges of RP perovskite materials while keeping their bandgap constant. Due to the electrostatic displacement of the band edge energy levels, excellent band alignment is achieved, the hole injection barrier is reduced and the charge balance within the emission layer is improved [55]. Bi-functional amphiphilic ions with different coordination affinities can coordinate with Pb^{2+}, shortening the distance of the quantum well and acting as co-spacer organic layers, to inhibit the aggregation of perovskite precursors, thereby limiting the growth of high-n phases and promoting the growth of low-n phases, and improving energy transfer [56].

Defect passivation is a commonly used strategy to reduce or eliminate non-radiative recombination defects in perovskites and thereby improve the device performance

[57, 58]. As shown in Fig. 2(d), the addition of crown ether and polyethylene glycol methyl ether acrylate can alter the crystal structure and passivate defects, leading to the high-quality, environmentally stable, and low-defect density perovskite films [5]. The dual additive treatment reduces the defect state density of the perovskite, resulting in an increase in the PL quantum yield from 12% to 78%. Also, introducing 2D perovskite and excess PEABr into the solution precursor of RP perovskites can significantly reduce the defect density, thus reducing the impact of non-radiative recombination [59]. Furthermore, when using a precursor combination of organic halide salts and 3D perovskites to prepare RP perovskite films, the organic ammonium cation not only passivates defects but also ensures the effective formation of high-order domains in the RP perovskites, avoiding the appearance of low-order domains [60]. In addition, modifying $CsPbBr_3$ nanocrystals with PEA bromide and introducing them into RP perovskite films can effectively modify the halide vacancies associated with excitonic non-radiative transitions and reduce the defect [61]. In addition to the passivation of internal defects in crystals, the passivation of interface defects is also of great significance in regulating emission properties. Recently, a functionalized phosphonic acid was developed as a passivating agent for the coordinating unsaturated Pb^{2+} defects without affecting the crystallinity of RP perovskites [62]. These agents were used to passivate the buried interfaces, fill in interface charge traps, and ultimately lead to high quantum efficiency [63].

3.4 Dimension and interface dependent emission properties

The optical properties of RP perovskites are affected by n as well as the physical size of RP perovskites. In small n, quantum confinement effects become more prominent, leading to higher exciton binding energies and stronger PL. For example, 4'-(aminomethyl)-biphenyl-3-carboxylic acid can be added to $PEA_2(FAPbBr_3)_2PbBr_4$ to promote the formation of large n-phases, while reducing van der Waals gaps between quasi 2D perovskite layers and enhancing interlayer coupling [64]. Alternatively, quasi-2D perovskite flat films with uniform 2D–3D phase mixtures can be prepared by dropping antisolvent containing nanocrystals into RP perovskite precursor solutions [65]. Additionally, iodide salts can be used as additives to induce the formation of iodide lead salts and increase monomer density [66]. Antisolvents are also used to control the n value. It has been found that a mixed antisolvent of ethyl acetate and isopropanol can effectively remove excess large organic ligands and suppress the growth of low-n phase RP perovskites [67]. By matching the temperature with the boiling point of the antisolvent, the solvent and antisolvent can be evaporated simultaneously, allowing perovskite microcrystals to nucleate uniformly along the circumference and significantly reducing the dispersion of the $n = 2$ perovskite phase, resulting in perovskite films with a narrow phase distribution [68].

The interface effect significantly influences the emission characteristics of RP perovskites. Charge-transfer excitons have been observed at the interface of PEA_2PbI_4–PEA_2SnI_4 heterostructures, which can be directly formed under electrical injection, advancing the functionalities of RP perovskites as white light sources [69]. Moreover, 2D perovskite lateral heterostructures were also realized by a quaternary solvent method, utilizing rigid π-conjugated organic ligands to avoid in-plane ion diffusion. The exciton lifetime is enhanced at the interface of the $(2T)_2PbBr_4$–$(2T)_2PbI_4$ heterostructure and the $(4Tm)_2SnI_4$–$(4Tm)_2PbI_4$ heterostructure, opening new avenues to tune the excitonic properties via lattice-strain engineering [70].

4 Amplified spontaneous emission of RP perovskites

4.1 Operation wavelength

Amplified spontaneous emission (ASE) is a phenomenon in which the amplification of spontaneous emission occurs when the optical gain exceeds the optical losses. An effective way to provide commercial value and demand guidance is to summarize the operation wavelengths of ASE. In this part, we will discuss the ASE from the RP perovskite and 2D–3D perovskites, and a summary of ASE wavelengths and thresholds is shown in Table 1. Li *et al.* [71] obtained ASE spectra with adjustable wavelengths ranging from 530 nm to 810 nm, under pulsed excitation using self-assembled $NMA_2(FA)_{n-1}Pb_nX_{3n+1}$ perovskites films [Fig. 3(a)]. Wang *et al.* [7] demonstrated blue ASE from the $CsPbCl_{1.5}Br_{1.5}$-based 2D–3D perovskite thin films. Ding *et al.* [72] reported that by utilizing ethanol to manage the solubility of perovskite precursors, high-quality single-crystal samples of $(TEA)_2(MA)_{n-1}Sn_nI_{3n+1}$ (where $n = 1$ or 2) were produced, exhibiting red ASE spectra at 674 nm and 754 nm, respectively. In summary, the ASE phenomenon in RP halide perovskites has covered a broad spectral range from near-infrared to blue, exhibiting great prospects for materials research and commercial applications.

4.2 Threshold

In recent years, extensive research has been conducted to investigate the ASE threshold of RP perovskite. The reduced threshold indicates reduced optical losses. RP perovskite is usually not a solitary phase but comprises a cluster of phases, and even exhibits different n values. Threshold analysis of RP perovskite films can effectively help to understand the PL efficiency in the spontaneous

Table 1 The ASE wavelengths and thresholds for RP perovskites.

Year	Materials	Structure	Pump	Temperature	Wavelength	Threshold	Ref.
2018	$NMA_2(FA)Pb_2Br_yI_{7-y}$ (y = 7, 4, 3, 2, 1 and 0)	thin film	pulsed	RT	530–810 nm	8.0 μJ·cm^{-2}	[71]
2021	$Cs_{0.87}(FAMA)_{0.13}PbBr_3/NMA_2PbBr_4$	thin film	pulsed	RT	530 nm	1.44 μJ·cm^{-2}	[74]
2021	$Cs_{0.87}(FAMA)_{0.13}PbBr_3/(NMA)_2PbBr_4$	thin film	pulsed	RT	535 nm	3.8 μJ·cm^{-2}	[84]
2022	$CsPbCl_{1.5}Br_{1.5}/(DPEA)_2PbBr_4$	thin film	pulsed	RT	468 nm	6.5 μJ·cm^{-2}	[7]
2022	$(ThMA)_2Cs_2Pb_3Br_{10}$	thin film	pulsed	RT	530 nm	13.92 μJ·cm^{-2}	[75]
2022	$(PEA)_2Cs_{n-1}Pb_nBr_{3n+1}$	thin film	pulsed	RT	525 nm	11.3 μJ·cm^{-2}	[80]
2022	$PEA_2Cs_4Pb_5Br_{16}$	thin film	pulsed	RT	535 nm	11.7 μJ·cm^{-2}	[81]
2022	$(TEA)_2(MA)_{n-1}Sn_nI_{3n+1}$ (n = 1, 2)	single crystal	pulsed	20 K	674–754 nm	29.1 μJ·cm^{-2}	[72]
2022	$(PEA)_2(MA)_{n-1}Pb_nI_{3n+1}$ (n = 1, 2, 3)	single crystal	pulsed	20 K	541–627 nm	5.8 μJ·cm^{-2}	[85]

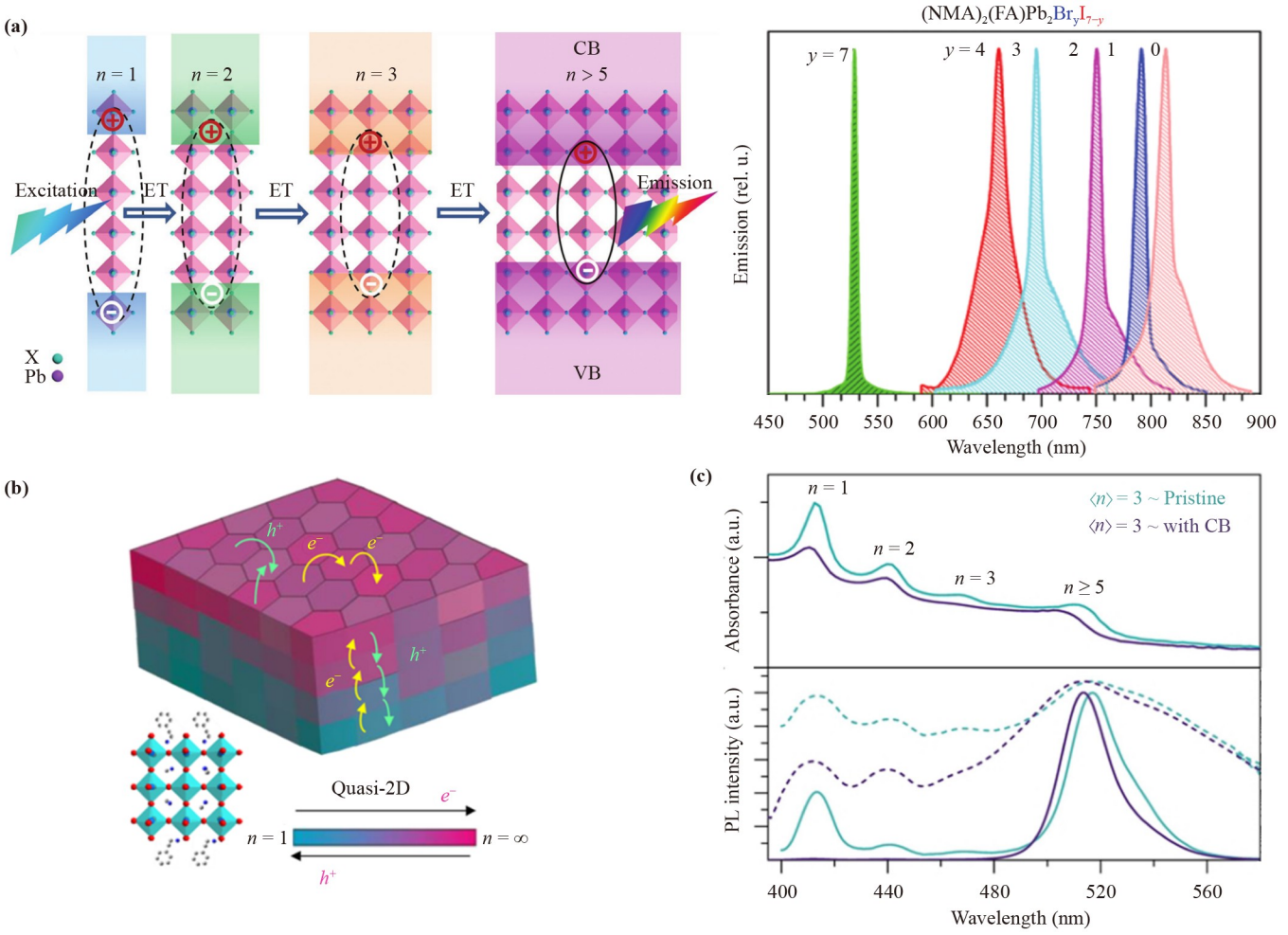

Fig. 3 Amplified spontaneous emission properties of RP perovskites are presented in this study. **(a)** Energy transfer cascades occur as small n-value wide-bandgap quantum wells transfer energy to large n-value narrow bandgap QW emitters. The 2D-RPP thin films $(NMA)_2(FA)Pb_2Br_yI_{7-y}$ (where y = 7, 4, 3, 2, 1, and 0) can emit ASE in a broad range of wavelengths by adjusting the precursor solutions. **(b)** A diagram displaying the electronic transitions in multiphase perovskite thin films is presented. **(c)** The impact of an anti-solvent on $(ThMA)_2Cs_2Pb_3Br_{10}$ films was studied. The PL peak shifts from 518 to 513 nm after CB treatment. (a) Reproduced from Ref. [71]. (b) Reproduced from Ref. [73]. (c) Reproduced from Ref. [75].

radiation process and provide a reference for the selection of optical devices [Fig. 3(b)][73]. However, the development of low-threshold, high-gain lasers using RP perovskite lags behind that of 3D perovskite. To address this issue, researchers have employed different methods to lower their ASE threshold. Liang *et al.* [74] proposed a technique involving solvent recrystallization that was employed to enhance the crystallinity of mixed-cation

$Cs_{0.87}(FAMA)_{0.13}PbBr_3/NMA_2PbBr_4$ films deposited through spin-coating, and to eliminate pinholes. The ASE threshold is reduced from 3.00 to 1.44 μJ·cm^{-2}, which can be ascribed to the relatively low propagation loss and suppressed Auger recombination. Qin *et al.* [75] synthesized $(ThMA)_2Cs_{n-1}Pb_nBr_{3n+1}$ films by a facile solvent method and optimized the phase distribution of the film by counteracting the solvent chlorobenzene, thus improving the energy transfer efficiency and achieving a low ASE threshold of 13.9 μJ·cm^{-2} [Fig. 3(c)]. In addition, modifying gain mechanisms can also regulate the performance of ASE [76]. Due to the higher recombination rate of multiexcitons than that of free excitons, Li *et al.* [77] achieved multiexciton ASE in $PEA_2(CH_3NH_3)_7Pb_8Br_{25}$ with grain size less than 1 μm, reaching a threshold as low as 13.7 μJ·cm^{-2} and almost half of that of ASE from free excitons. These studies demonstrate that the ASE phenomenon in RP perovskites has significant potential for materials research and commercial applications.

4.3 Gain dynamics

To enhance the optical gain of RP perovskite materials, researchers have employed various approaches to enhance the efficiency of energy transfer and minimize the loss of energy through non-radiative pathways. Yang *et al.* [78] increased the content of 3D phase in the RP perovskite by introducing hypophosphoric acid, which improved the crystallinity, charge transport, and energy funneling process, leading to efficient luminescence. Allegro *et al.* [79] introduced silicon substrates to eliminate the waveguide effect in RP perovskite films, alter the lattice structure and eliminate lattice mismatch, resulting in more effective charge and energy transfer, reducing non-radiative recombination and increasing the intensity of optical gain. In the work of Huang *et al.* [80], the addition of polyvinylpyrrolidone improved the energy funneling process, reduced non-radiative recombination and increased the optical gain by more than two times [Fig. 4(a)]. Li *et al.* [81] proposed a method that employs treatment with chlorobenzene, which is resistant to solvents, to control the phase composition and surface morphology of quasi-2D $PEA_2(CsPbBr_3)_{n-1}PbBr_4$ films [Fig. 4(b)]. These research works broaden the fundamental comprehension of the behavior of charge carriers in quasi-2D perovskite films [82].

4.4 Dimension and interface dependent ASE

Through dimension and interface control at the molecular level, ASE can be effectively modulated. Li *et al.* [83] decreased the spacer content and utilized NMA cation linkers to maximize the volume fraction of the large n value quantum well, which suppresses exciton–exciton annihilation and lowers the ASE threshold. Besides, Li *et al.* [84] employed a multi-cation doping strategy to prepare a dense and smooth $Cs_{0.87}(FAMA)_{0.13}PbBr_3/(NMA)_2PbBr_4$ film [Fig. 4(c)]. The addition of NMA cations reduced the grain size, resulting in a highly smooth film and introducing an energy diagram similar to a quantum well to increase the exciton oscillation strength and promote optical gain [84]. These methods effectively enhance the optical properties of quasi-two-dimensional perovskite films and have important implications for the application of luminescent materials.

5 Photonic lasing of RP halide perovskites

5.1 VCSEL

VCSELs, or vertical-cavity surface-emitting lasers, represent a promising new type of optoelectronic device. They are composed of multiple layers of semiconductor materials and a substrate layer, which generate laser light through vertical reflection and resonance within the cavity. Compared to traditional edge-emitting lasers, VCSELs have several advantages, including ease of integration, low processing costs and high yield. Wang *et al.* [7] employed 2,2-diphenylethylammonium bromide as a binding agent to form RP perovskite thin films with increased distribution for large n value domains [Fig. 5(a)]. By concentrating photogenerated carriers on high-n regions, it is possible to reduce the local carrier density and effectively suppress Auger recombination. This presents a viable approach to regulate the spatial arrangement of RP perovskite VCSEL domains. Chu *et al.* [86] proposed a flexible and large-area thin film transfer technique that was employed to extend the cavity through resonance conditions. They used alkali halide NaBr to prepare a smooth and highly luminescent RP perovskite thin film $(PEA)_2Cs_{n-1}Pb_nX_{3n+1}$ (X = Br, Cl), Afterward, the film with a large area was moved to the ultimate substrate. Based on this, they achieved a low-threshold, high-quality single-mode VCSEL. These technological developments provide effective ways to achieve RP perovskite VCSELs with potential for future applications.

5.2 DFB Laser

Distributed feedback (DFB) lasers are a type of edge-emitting semiconductor laser that employs a feedback structure created by doping or suppression in the active layer to produce periodic refractive index modulation. As mirrorless, high-speed and single-mode lasers, DFB cavities hold tremendous potential for applications in spectroscopy and long-distance optical communication. To investigate whether the single-state-to-triplet-state exciton annihilation induced by triexcitons hinders the population inversion in RP perovskites, Qin *et al.* [87] studied two types of organic cations, PEA with high

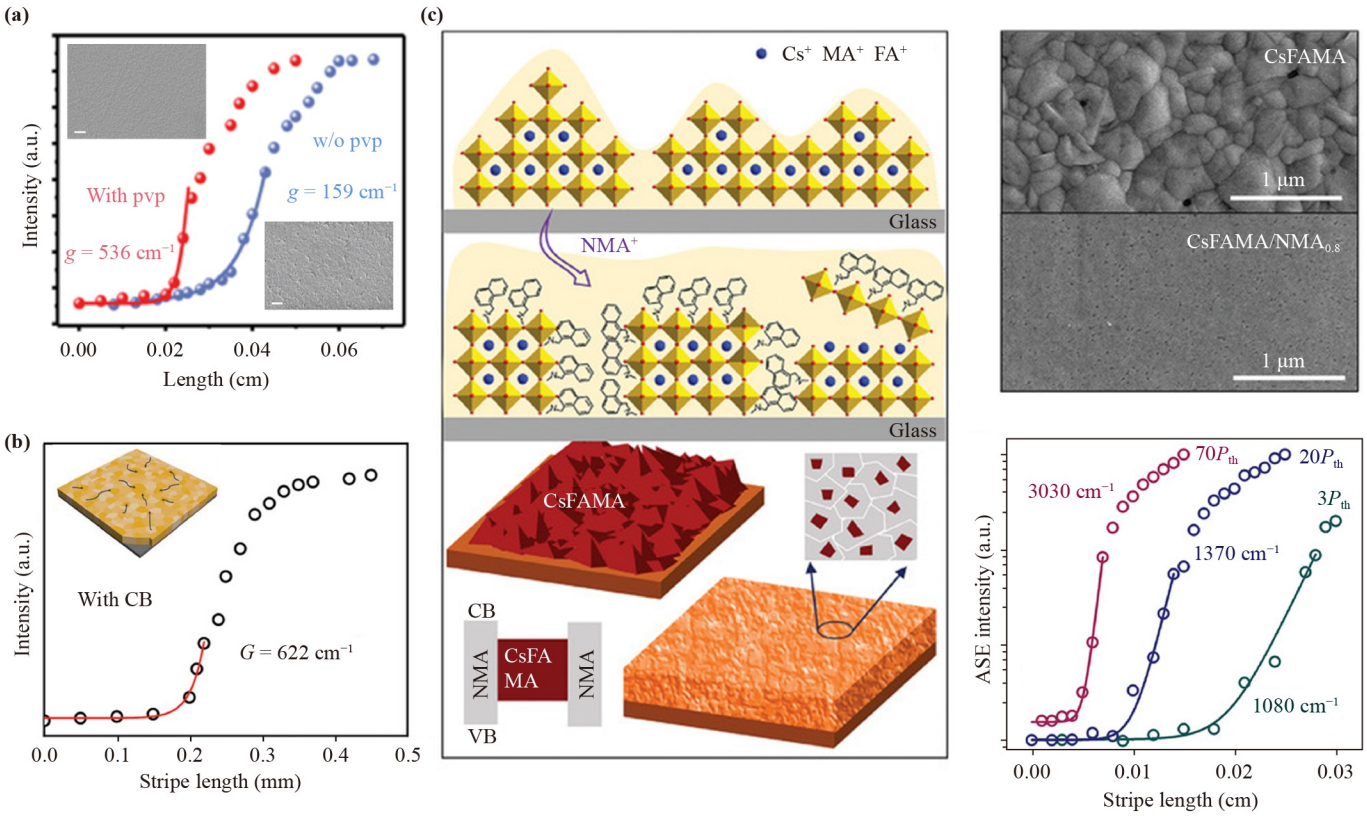

Fig. 4 Ways to control the gain of RP perovskites. **(a)** The output intensity's correlation with stripe length is demonstrated for both the untreated perovskite film and the PVP-modified perovskite film. **(b)** The film subjected to CB treatment exhibits a net gain coefficient of 622 cm^{-1}. **(c)** The above is a mixed cation doping strategy, where the addition of long-chain NMA cations hinders the growth of perovskite grains by inhibiting their surface self-assembly. Meanwhile, the film morphology of CsFAMA and CsFAMA/$NMA_{0.8}$ perovskites is shown, as well as their SEM images. In addition, the integrated 1PP-ASE intensity of the CsFAMA/$NMA_{0.8}$ film is described. (a) Reproduced from Ref. [80]. (b) Reproduced from Ref. [81]. (c) Reproduced from Ref. [84].

triplet energy and NMA with low triplet energy, were utilized in $FAPbBr_3$-based RP perovskites [Fig. 5(b)]. By employing a high-quality factor distributed feedback cavity and trion management strategy, the researchers achieved stable lasing in continuous wave mode at room temperature, with NMA-based films exhibiting lower threshold. Lei *et al.* [88] prepared highly oriented quasi-2D perovskite $(PEA)_2(FA)_3Pb_4Br_{13}$ films relying on solution engineering with N-methyl-2-pyrrolidone and dimethyl sulfoxide. Their research revealed that the film demonstrated accelerated energy transfer from regions with high bandgap to those with low bandgap compared to films with random orientation, facilitating the low-threshold DFB lasers.

5.3 Microlaser and Nanolaser

Perovskite microlasers have gained importance in optoelectronics due to their compact size, low energy consumption, low operating voltage, and ability to emit light in both visible and infrared spectra [89]. Specific functions of perovskite microlasers can be achieved through the design and processing of microcavities. Liang *et al.* [90] discovered the laser and loss mechanisms of two-dimensional $(BA)_2(MA)_{n-1}Pb_nI_{3n+1}$ microplatelets that were mechanically exfoliated from bulk crystals [Fig. 5(c)]. As n decreases from 5, 4 to 3, the laser threshold exhibits a significant increase, while the characteristic temperature decreases to 49 K, 25 K, and 20 K for the corresponding samples. The dependence of lasing behavior on the value of n is attributed to the decreased Auger recombination rate and electron-phonon coupling strength with increasing n, which provides insights for the development of two-dimensional semiconductor microlasers with low threshold, no substrate and multiple colors. He *et al.* [85] used a straightforward method for growing to prepare single crystal flakes of $(PEA)_2(MA)_{n-1}Pb_nI_{3n+1}$ (n = 1, 2, 3), which produced low-threshold amplified spontaneous emission. These results enriched an understanding of the interactions between many-body excitons at a fundamental level in layered perovskites and provided insights for the development of solution-processed multi-color microlasers. Gao *et al.* [91] studied at low temperatures (≤153 K),

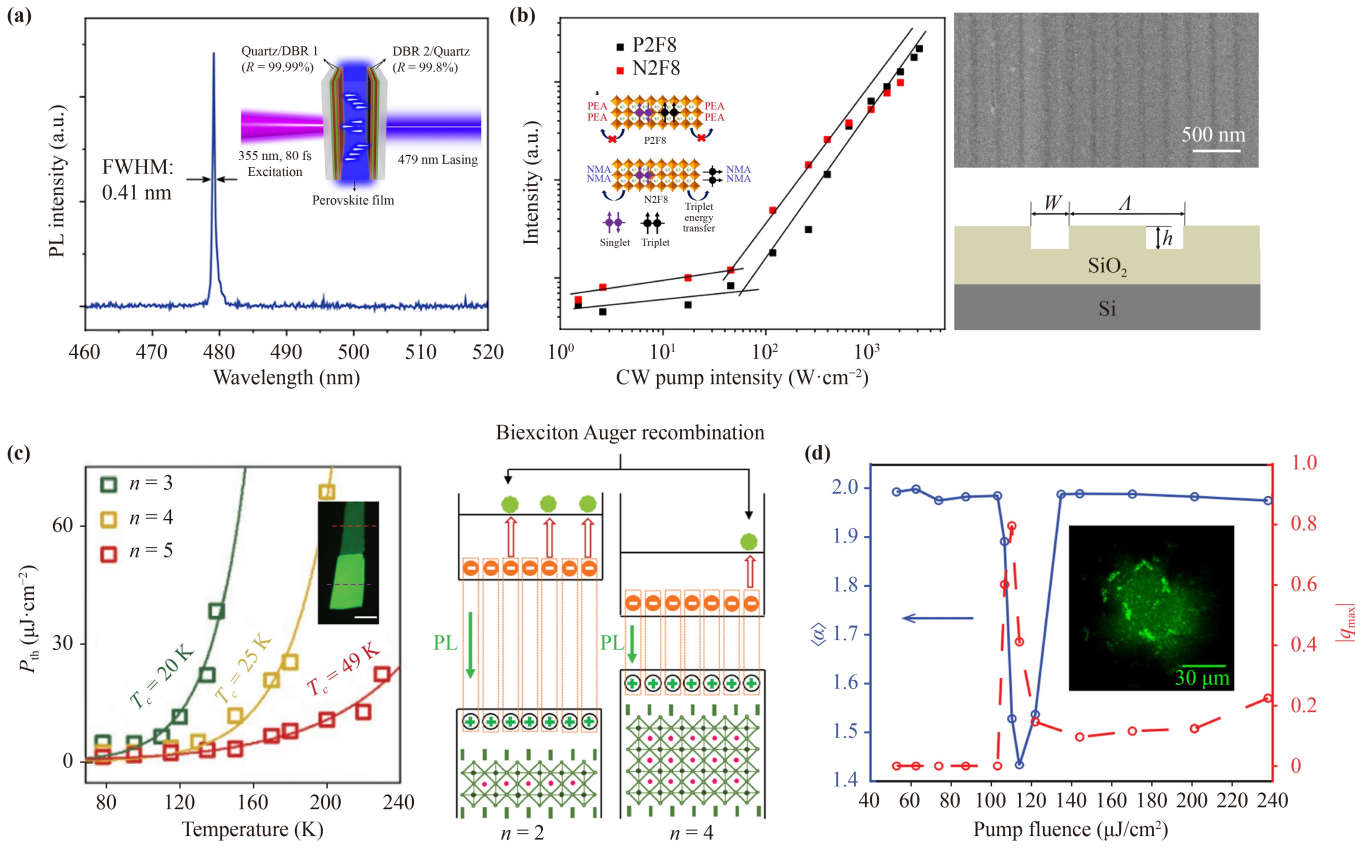

Fig. 5 RP perovskite laser. **(a)** A schematic diagram of a vertical-cavity surface-emitting laser is shown, with a corresponding PL spectrum. **(b)** This depicts the DFB resonator structure with an air-trench width of 120 nm, a grating period of 250 nm and a grating height of 60 nm. Additionally, a top-down SEM image and a graph showing the relationship between laser intensity and pump intensity are presented. **(c)** A PL image is presented to display the as-exfoliated $n = 1$ RP perovskite microflakes, followed by the biexciton Auger recombination process. The plot displays the variation of lasing thresholds for $n =$ 3, 4, and 5 RP perovskites as a function of temperature, represented by data points. As the value of n decreases, the lasing threshold exhibits an upward trend. **(d)** A lasing image of the PEABr-FAPbBr$_3$ perovskite film. (a) Reproduced from Ref. [7]. (b) Reproduced from Ref. [87]. (c) Reproduced from Ref. [90]. (d) Reproduced from Ref. [93].

homogeneous mechanically-exfoliated $(PEA)_2(MA)_{n-1}Pb_nI_{3n+1}$ ($n = 2$, 3) microflakes exhibit up-conversion lasing in the 598– 637 nm wavelength range. The low lasing threshold is due to their high two-photon absorption coefficients, nearly 3 orders of magnitudes higher than their 3D counterparts [91]. These characteristics make RPP a potential gain medium for developing high-efficiency up-conversion microcavity lasers.

5.4 Random laser

Random lasers are a type of laser whose laser mode is not achieved through traditional reflection and resonance, but rather through the scattering of photons in the random microstructure of materials [92]. Compared to traditional lasers, random lasers have irregular resonant cavities, simple preparation, low cost, controllable morphology and easy modulation, making them potentially useful in multiple fields such as optical imaging and biomedicine. Fruhling *et al.* [93] have shown the random lasing and potential coherent feedback mechanisms of RP perovskite thin films [Fig. 5(d)]. The lasing modes are extended states caused by random grain structures in the solution processing that can span the entire pump volume. Also, Roy *et al.* [94] produced a FA-(N-MPDA) $PbBr_4$ hybrid perovskite with high quality by employing a constant temperature slow evaporation approach with the aid of a long-chain organic diamine spacer. By utilizing the defects and dislocations as well as grain boundaries as scattering centers, they achieved a low-threshold random laser in the well-shaped high-crystallinity nanorods, with extremely small spectral width (~0.1 nm) and high Q-factor (~5350). These results suggest the great potentials of RP perovskite random lasing.

6 Polaritonic lasing of RP perovskites

6.1 Exciton–polaritons in linear regime

Exciton–polaritons (polaritons for short) are part-matter,

part-light quasiparticles formed from the superposition of the semiconductor excitons and cavity photon modes with sufficiently strong interaction [95]. Embedding the 2D layered perovskites in an external optical cavity with two distributed Bragg reflectors, or one DBR and one metallic mirror constructs the most used configurations to achieve strong exciton–photon coupling [Fig. 6(a)] [96]. Benefitting from the high-quality F–P cavity and large exciton binding energies, polaritons can be easily formed, where a clear anticrossing characteristic and a large vacuum Rabi splitting energy of approximately 170 meV could be distinguished. Meanwhile, hybridized polariton states were observed in 2D organic–inorganic perovskite planar microcavities, deriving from a significant coherent strong coupling of 2D perovskite exciton, multimode cavity modes and Bragg modes of the distributed Bragg reflector and the reversible energy oscillation between the three states [Fig. 6(b)] [97]. On the other hand, recent research has unveiled the strong exciton–photon coupling in 2D layered perovskite flakes at room temperature even without external cavities, as shown in Fig. 6(c) [96]. The strong polariton nonlinearities in those single-crystal flakes, manifested as excitonic interaction constants reaching the highest level at room temperature (~3 ± 0.5 μeV·μm^2), are hundreds of times higher than those in inorganic semiconductors at cryogenic temperatures. Moreover, single-cavity polaritons with a Rabi splitting twice as large were observed by preparing a 2D layered perovskite with a thickness of about 150 nm on a gold substrate [98]. The coupling strength and order of exciton-polariton resonance in this structure are both functions of crystal thickness, and the splitting energy of polaritons is also linearly related to the thickness of the perovskite.

Furthermore, 2D layered perovskite microcavities offer a unique platform for investigating artificial non-Abelian gauge potentials and topological polariton physics due to their exceptional in-plane optical anisotropy and tunability with external factors such as electric field, temperature, and magnetic field. Specifically, there is a strong electric field in the two-dimensional layered perovskite microcavity. When an external light field exists in the microcavity, photons will be induced to deflect by a strong electric field, equivalent to introducing an artificial non-Abelian gauge field. The size and direction of this electric field can be tuned by external factors such as electric field, temperature, and magnetic field [99]. Using this controllable external field to break the time-reversal symmetry and combined with the optical spin–orbit coupling, the distribution of Berry curvature can be altered, leading to a non-zero integrated value, which allows for the control of its topological properties and this has practical applications in photonics as well as quantum information processing. A recent method has been proposed to electrically adjust the photonic Berry curvature of 2D layered perovskite microcavities, as shown in Fig. 6(d) [100]. The optical system consists of a liquid crystal cavity and a RP perovskite layer, which enables strong coupling between cavity photons and excitons, creating polaritons. By varying the external electric field, the symmetry of the liquid crystal cavity can be reduced, causing a gap to open at the polariton dispersion relation corresponding to the polar Dirac point. This allows for the local manipulation of the concentration of Berry curvature by applying an external voltage. Furthermore, as shown in Fig. 6(e), changing the external temperature and magnetic field strength can also achieve the distribution of Berry curvature [99]. This is due to the breaking of time-reversal symmetry by an external magnetic field, which increases the degeneracy of the diabolical point and thus obtains a non-zero integrated value of Berry curvature.

Additionally, 2D layered perovskites incorporated into open cavity architectures also display a pronounced exciton-photon coupling effect, enabling further control over the coupling strength and influencing the emission characteristics via the photonic component. As shown in Fig. 6(f), the coupling strength can be modulated and polarization control can be achieved by varying the thickness of the perovskite film in the cavity structure [101]. This cavity structure is prepared by coating an Al NP lattice on a $(PA)_2(MA)Pb_2I_7$ thin film. Additional ultrafast energy transfer pathways in the open cavity also lead to a polariton lifetime that is half that of the original exciton. Additionally, by coupling the photon Bloch modes of 2D layered perovskite rod-like lattices with the excitons, the regulation of exciton polariton dispersion at room temperature has been achieved [Fig. 6(g)] [102]. It is possible to design polar dispersion with linear, parabolic, and multi-valued characteristics by adjusting the photon Bloch modes coupled with the perovskite excitons. Finally, topological singularities can be used to control the emission of 2D perovskites in strong coupling regime [103]. As depicted in Fig. 6(h), the RP perovskite films prepared by spin-coating on quartz substrates with triangular patterns exhibit circularly polarized eigenstates with topological polarization singularity. This symmetrically broken triangular structure shows strong emission enhancement and a larger circular polarization of about 0.835, due to the transfer of lower polariton branches to the low-loss spectral region in a strong coupling regime.

6.2 Exciton–polariton condensation and lasing

As light–matter hybrid bosonic quasiparticles, exciton polaritons exhibit remarkable potential for realizing Bose-Einstein condensation, forming a macroscopically-occupied quantum-degenerate phase with spontaneous coherence without the need for population inversion, which can serve as a novel low-threshold coherent light source called polariton lasing [104]. Although polariton conden-

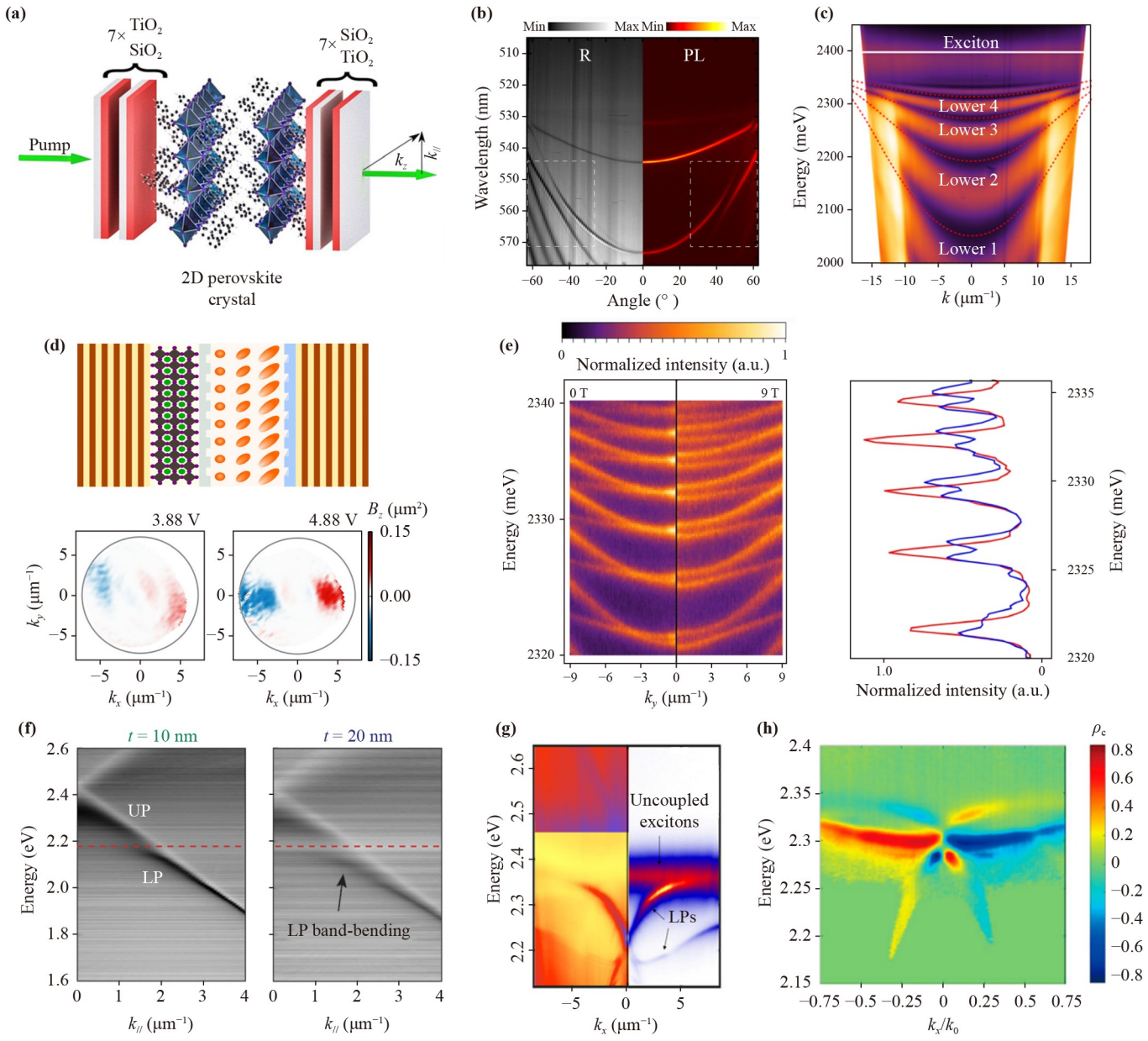

Fig. 6 **(a)** Schematic diagram of embedding RP perovskite single crystals in an optical cavity formed by two DBRs. **(b)** Angle-resolved reflectivity spectra (left panel) and angle-resolved PL (right panel) spectra of 2D perovskite microcavity. **(c)** Angle-resolved reflectivity spectra of a PEAI crystal slab. **(d)** Schematic diagram of 2D polycrystalline perovskite microcavity with liquid crystal and experimental B_z distribution of low energy modes as a function of voltage. **(e)** The relationship between the energy of non-polarized PL and the momentum in the k_y plane in the $B = 0$ T magnetic field (left) and the $B = 9$ T external magnetic field (right) when $T = 4$ K; The red and blue lines represent the PL spectra measured at zero magnetic field and $B = 9$ T for $k_x = 0$ μm^{-1}, $k_y = 3.7$ μm^{-1}, respectively. **(f)** Experimental angle-resolved transmission of lattices with film thicknesses of 10 nm and 20 nm under s-polarized light. **(g)** Experimental results of the angle-resolved reflectivity spectra (left panels) and the angle-resolved PL response (right panels). **(h)** Degree of circular polarization of triangular patterns in the Fourier plane. (a, c) Reproduced from Ref. [96]. (b) Reproduced from Ref. [97]. (d) Reproduced from Ref. [100]. (e) Reproduced from Ref. [99]. (f) Reproduced from Ref. [101]. (g) Reproduced from Ref. [102]. (h) Reproduced from Ref. [103].

sation at room temperature has been extensively achieved in 3D inorganic perovskite microcavities, it remains challenging to achieve in 2D and RP perovskite microcavities owing to the relatively lower cavity quality factor and the inevitable presence of defects or grain boundaries resulting in poor material quality.

In 2020, polariton condensation was demonstrated in a 2D RP single-crystal perovskite microcavity under

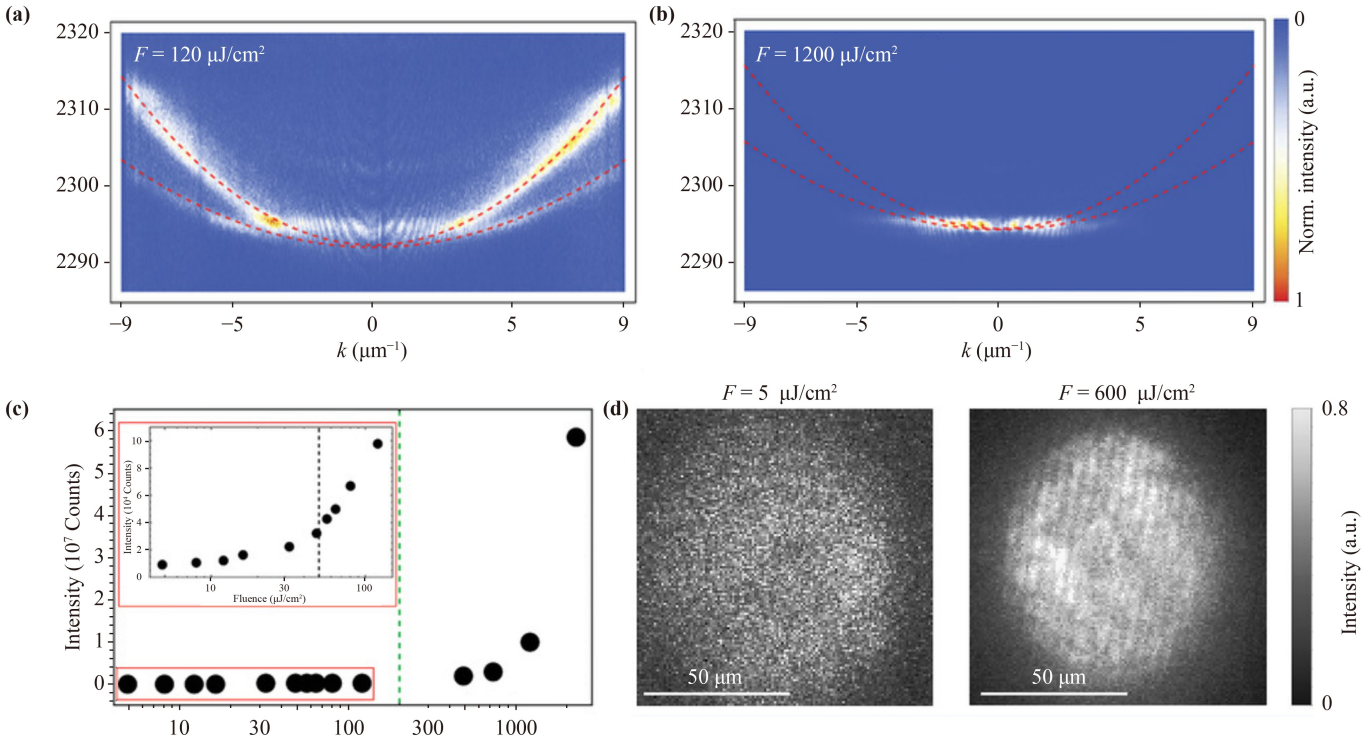

Fig. 7 **(a, b)** Energy and momentum emission intensity diagrams of perovskite single crystals excited by two different incident pump fluxes. At 120 μJ/cm^2, that is, between two thresholds, exhibits bi-exciton laser emission. At 1200 μJ/cm^2, that is, above the second threshold, the emission collapses to the bottom of polariton dispersion and the bi-exciton emission stops, forming a polariton condensate. **(c)** The integral intensity of emission varies with the incident pump flux. Inset: enlarged view of weak excitation region.The black dashed line represents the first threshold, and the green dashed line represents the second threshold. **(d)** Real spatial emission map for two different incident pump fluxes. At 5 μJ/cm^2, i.e., below the first threshold, there are no interference fringes present. At 600 μJ/cm^2, i.e., above the second threshold, a macroscopic coherent state with interference fringes above 50 μm × 50 μm appears. (a–d) Reproduced from Ref. [105].

femtosecond pulsed excitation at cryogenic temperature (4 K) [105]. The microcavity was composed of a top silver mirror and a bottom DBR, in which a benzylammonium lead iodide perovskite single crystal was embedded. As depicted in Fig. 7(c), two distinct thresholds were observed, ascribing to the onset of lasing from biexcitons and polariton condensation, respectively [Figs. 7(a) and (b)]. Above the second threshold, the entire emission collapsed to a lower energy state and a polariton condensate was formed at the bottom of the lower polariton branch. The collapse of the lower polariton diffusion leads to its minimum value, resulting in the cessation of biexciton emission and a sudden increase in the total emission intensity, establishing a macroscopic coherent state with a spatial coherence over 50 μm × 50 μm, as shown in Fig. 7(d). Notably, only high-quality samples without disorders exhibit two distinct thresholds, highlighting the importance of eliminating structural defects.

To date, there have been no reliable reported demonstrations of room-temperature polariton condensation in RP halide perovskites and even at cryogenic temperatures, the condensation threshold remains quite high. Although excitons in RP perovskites are more stable than those in 3D perovskites, there are still other factors that influence the formation of polariton condensates in RP perovskites. For instance, nonradiative recombination associated with defects or grain boundaries can shorten the exciton lifetime in RP halide perovskites, reduce the chance of polariton formation, and hinder the polariton scattering process [14]. Temperature effects also may increase the thermal motion of excitons and photons in RP perovskites, shortening the time they interact with each other and thus limiting the formation of polaritons.

7 Challenges and perspective

As seen from the preceding sections, RP perovskite materials are a class of materials with excellent optoelectronic properties, which can be considered as heterojunctions of pure 2D RP perovskite and 3D halide perovskite. They exhibit stronger carrier confinement, larger exciton binding energy, and higher stability compared to traditional 3D halide perovskites [13, 106, 107]. These results have enriched the field of laser research, indicating a

broad development prospect for RP perovskite materials. However, RP perovskites also have limitations compared to traditional 3D perovskites. Firstly, from a structural perspective, the physical stability of RP perovskites is poor because the weak interlayer interactions lead to a loose structure and the lack of support from a three-dimensional structure [108]. Therefore, it is necessary to find organic cations with stronger conjugation as interlayer spacers to enhance interlayer interactions. Alternatively, other 2D perovskite structures such as the DJ or ACI structure can be studied to enhance interlayer interaction by changing the connection configuration between organic layers. Secondly, unlike 3D perovskites, multiple phases inevitably form in the solution-processed fabrication methods, which enables the cascade energy transfer. Since low-n phase suffers from strong electron-phonon coupling and Auger recombination and induces inefficient carrier transfer, some progress has been made to control the phase distribution and optimize the ASE/laser performance [82, 90, 109]. Inspired by these works, precise control of phase distribution is waiting to be developed.

The polaritons formed in RP perovskites play an important role in enhancing the optoelectronic properties. In terms of optical properties, polaritons can enhance the absorption and emission intensity of RP perovskites and cause blue shift in emission [95]. However, research on polaritons in RP perovskites still faces significant challenges. First, the physical nature of polaritons in RP perovskites is not well understood. Although some research on polaritons in RP perovskites has been conducted, there is still controversy and uncertainty about the physical nature of these excitons, requiring further theoretical research and experimental verification. Second, RP perovskites have weak stacking interactions and high surface energy, which make polaritons prone to aggregation and decomposition during preparation and application [110, 111]. Therefore, rational chemical modification and material design are needed to improve their stability. Additionally, achieving effective control over polaritons in RP perovskite materials remains an important challenge. Rational material and device structure design is needed to achieve polaritons modulation in perovskite materials for better application potential in optoelectronic devices. Finally, as a new type of excited state, polaritons have potential applications in optoelectronic devices [105]. However, the application of polariton lasing in RP perovskite materials is still in the exploratory stage, requiring further research on their potential in areas such as optical switches, sensors, and quantum computing [112, 113].

Further, electrically-pumped lasing has always been the eternal goal. To date, the green and red CW pumped lasing of RP perovskites has been realized in a DFB cavity. Meanwhile, electrically-driven high-yield light emitting diodes were also reported for the RP perovskites. Thus, it is very timely to design electrically-pumped lasing devices. Exploring the photophysics of excitons and other types of carriers under strong excitation, gain medium-cavity interface engineering, and device configurations should be helpful. Similarly, we can optimize the performance of perovskite lasers through various means, such as improving the quality of perovskite crystals during the preparation process, optimizing the laser structure, doping with different metal ions, and controlling temperature to increase heat dissipation and enhance stability. More fundamentally, the development of physical mechanisms will add up possibilities for 2D perovskite lasers, including trion gain and optical gain enhancement by exciton–polariton [76, 114–116]. Additionally, we can refer to researches on size and interface engineering in the fields of LEDs and perovskite solar cells, designing passivators to balance carrier confinement and transfer, doping with organic cations to passivate perovskite defects, etc. [10, 117, 118]. These reports have produced highly stable perovskites, but have not been extensively explored in laser devices. With the development of perovskite device technology, we believe that more feasible operation techniques will be obtained, and these challenges will be successfully addressed.

Declarations The authors declare that they have no competing interests and there are no conflicts.

Acknowledgements Q. Z. acknowledges the funding support from the National Natural Science Foundation of China (Nos. 52072006 and 51991344) and the Natural Science Foundation of Beijing Municipality (No. JQ21004). F. L. acknowledges the funding support from the Hubei Province Science and Technology Major Project (No. 2022AAA008), the National Natural Science Foundation of China (No. 12374319), and the Knowledge Innovation Program of Wuhan-Basic Research (No. 2022010801010349). S. C. acknowledges the funding support from the Macau Science and Technology Development Fund (Nos. FDCT-0096/2020/A2 and FDCT-0082/2022/A2).

References

1. L. Zhang, C. Sun, T. He, Y. Jiang, J. Wei, Y. Huang, and M. Yuan, High-performance quasi-2D perovskite light-emitting diodes: From materials to devices, *Light Sci. Appl.* 10(1), 61 (2021)
2. Z. Wang, F. Wang, W. Sun, R. Ni, S. Hu, J. Liu, B. Zhang, A. Alsaed, T. Hayat, and Z. Tan, Manipulating the trade-off between quantum yield and electrical conductivity for high-brightness quasi-2D perovskite light-emitting diodes, *Adv. Funct. Mater.* 28(47), 1804187 (2018)
3. Q. Sun, Z. Fang, Y. Zheng, Z. Yang, F. Hu, Y. Yang, W. Yang, X. Hou, and M. H. Shang, Regulating the phase stability and bandgap of quasi-2D Dion–Jacobson $CsSnI_3$ perovskite via intercalating organic cations, *J. Mater. Chem. A* 10(8), 3996 (2022)

4. A. Jana, Q. Ba, and K. S. Kim, Compositional and dimensional control of 2D and quasi-2D lead halide perovskites in water, *Adv. Funct. Mater.* 29(28), 1900966 (2019)
5. Z. Liu, W. Qiu, X. Peng, G. Sun, X. Liu, D. Liu, Z. Li, F. He, C. Shen, Q. Gu, F. Ma, H. L. Yip, L. Hou, Z. Qi, and S. J. Su, Perovskite light-emitting diodes with EQE exceeding 28% through a synergetic dual-additive strategy for defect passivation and nanostructure regulation, *Adv. Mater.* 33(43), 2103268 (2021)
6. Y. Ji, M. She, X. Bai, E. Liu, W. Xue, Z. Zhang, K. Wan, P. Liu, S. Zhang, and J. Li, In-depth understanding of the effect of halogen-induced stable 2D bismuth-based perovskites for photocatalytic hydrogen evolution activity, *Adv. Funct. Mater.* 32(31), 2201721 (2022)
7. C. Wang, G. Dai, J. Wang, M. Cui, Y. Yang, S. Yang, C. Qin, S. Chang, K. Wu, Y. Liu, and H. Zhong, Low-threshold blue quasi-2D perovskite laser through domain distribution control, *Nano Lett.* 22(3), 1338 (2022)
8. Z. Li, E. Hong, X. Zhang, M. Deng, and X. Fang, Perovskite-type 2D materials for high-performance photodetectors, *J. Phys. Chem. Lett.* 13(5), 1215 (2022)
9. J. C. Hu, X. L. Wen, and D. H. Li, Optical properties of two-dimensional perovskites, *Front. Phys.* 18(3), 33602 (2023)
10. H. Lai, D. Lu, Z. Xu, N. Zheng, Z. Xie, and Y. Liu, Organic-salt-assisted crystal growth and orientation of quasi-2D Ruddlesden–Popper perovskites for solar cells with efficiency over 19%, *Adv. Mater.* 32(33), 2001470 (2020)
11. S. Ramesh, D. Giovanni, M. Righetto, S. Ye, E. Fresch, Y. Wang, E. Collini, N. Mathews, and T. C. Sum, Tailoring the energy manifold of quasi-two-dimensional perovskites for efficient carrier extraction, *Adv. Energy Mater.* 12(10), 2103556 (2022)
12. H. Zheng, G. Liu, L. Zhu, J. Ye, X. Zhang, A. Alsaedi, T. Hayat, X. Pan, and S. Dai, The effect of hydrophobicity of ammonium salts on stability of quasi-2D perovskite materials in moist condition, *Adv. Energy Mater.* 8(21), 1800051 (2018)
13. K. Wang, C. Wu, D. Yang, Y. Jiang, and S. Priya, Quasi-two-dimensional halide perovskite single crystal photodetector, *ACS Nano* 12(5), 4919 (2018)
14. Z. Chen, Y. Guo, E. Wertz, and J. Shi, Merits and challenges of Ruddlesden–Popper soft halide perovskites in electro-optics and optoelectronics, *Adv. Mater.* 31(1), 1803514 (2019)
15. W. Bi, Q. Cui, P. Jia, X. Huang, Y. Zhong, D. Wu, Y. Tang, S. Shen, Y. Hu, Z. Lou, F. Teng, X. Liu, and Y. Hou, Efficient quasi-two-dimensional perovskite light-emitting diodes with improved multiple quantum well structure, *ACS Appl. Mater. Interfaces* 12(1), 1721 (2020)
16. X. Sheng, Y. Li, M. Xia, and E. Shi, Quasi-2D halide perovskite crystals and their optoelectronic applications, *J. Mater. Chem. A* 10(37), 19169 (2022)
17. S. Q. Luo, J. F. Wang, B. Yang, and Y. B. Yuan, Recent advances in controlling the crystallization of two-dimensional perovskites for optoelectronic device, *Front. Phys.* 14(5), 53401 (2019)
18. X. Lian, H. Wu, L. Zuo, G. Zhou, X. Wen, Y. Zhang, G. Wu, Z. Xie, H. Zhu, and H. Chen, Stable quasi-2D perovskite solar cells with efficiency over 18% enabled by heat–light co-treatment, *Adv. Funct. Mater.* 30(48), 2004188 (2020)
19. C. Zuo, A. D. Scully, D. Vak, W. Tan, X. Jiao, C. R. McNeill, D. Angmo, L. Ding, and M. Gao, Self-assembled 2D perovskite layers for efficient printable solar cells, *Adv. Energy Mater.* 9(4), 1803258 (2019)
20. C. Zuo, A. D. Scully, and M. Gao, Drop-casting method to screen Ruddlesden–Popper perovskite formulations for use in solar cells, *ACS Appl. Mater. Interfaces* 13(47), 56217 (2021)
21. P. S. C. Schulze, K. Wienands, A. J. Bett, S. Rafizadeh, L. E. Mundt, L. Cojocaru, M. Hermle, S. W. Glunz, H. Hillebrecht, and J. C. Goldschmidt, Perovskite hybrid evaporation / spin coating method: from band gap tuning to thin film deposition on textures, *Thin Solid Films* 704, 137970 (2020)
22. J. X. Zhong, W. Q. Wu, L. Ding, and D. B. Kuang, Blade-coating perovskite films with diverse compositions for efficient photovoltaics, *Energy Environ. Mater.* 4(3), 277 (2021)
23. B. Turedi, V. Yeddu, X. Zheng, D. Y. Kim, O. M. Bakr, and M. I. Saidaminov, Perovskite single-crystal solar cells: going forward, *ACS Energy Lett.* 6(2), 631 (2021)
24. M. Li, S. Bhaumik, T. W. Goh, M. S. Kumar, N. Yantara, M. Grätzel, S. Mhaisalkar, N. Mathews, and T. C. Sum, Slow cooling and highly efficient extraction of hot carriers in colloidal perovskite nanocrystals, *Nat. Commun.* 8(1), 14350 (2017)
25. K. Wang, J. Y. Park, Akriti, and L. Dou, Two-dimensional halide perovskite quantum-well emitters: A critical review, *EcoMat* 3(3), e12104 (2021)
26. Y. Liu, H. Ye, Y. Zhang, K. Zhao, Z. Yang, Y. Yuan, H. Wu, G. Zhao, Z. Yang, J. Tang, Z. Xu, and S. Liu, Surface-tension-controlled crystallization for high-quality 2D perovskite single crystals for ultrahigh photodetection, *Matter* 1(2), 465 (2019)
27. V. Naresh and N. Lee, Zn(II)-doped cesium lead halide perovskite nanocrystals with high quantum yield and wide color tunability for color-conversion light-emitting displays, *ACS Appl. Nano Mater.* 3(8), 7621 (2020)
28. B. Park, S. M. Kang, G. W. Lee, C. H. Kwak, M. Rethinasabapathy, and Y. S. Huh, Fabrication of $CsPbBr_3$ perovskite quantum dots/cellulose-based colorimetric sensor: Dual-responsive on-site detection of chloride and iodide ions, *Ind. Eng. Chem. Res.* 59(2), 793 (2020)
29. X. Cao, L. Zhi, Y. Jia, Y. Li, K. Zhao, X. Cui, L. Ci, D. Zhuang, and J. Wei, A review of the role of solvents in formation of high-quality solution-processed perovskite films, *ACS Appl. Mater. Interfaces* 11(8), 7639 (2019)
30. C. R. Kagan, L. C. Bassett, C. B. Murray, and S. M. Thompson, Colloidal quantum dots as platforms for quantum information science, *Chem. Rev.* 121(5), 3186 (2021)
31. Y. Liu, M. Siron, D. Lu, J. Yang, R. dos Reis, F. Cui,

M. Gao, M. Lai, J. Lin, Q. Kong, T. Lei, J. Kang, J. Jin, J. Ciston, and P. Yang, Self-assembly of two-dimensional perovskite nanosheet building blocks into ordered Ruddlesden–Popper perovskite phase, *J. Am. Chem. Soc.* 141(33), 13028 (2019)

32. L. Zhao, P. Tang, D. Luo, M. I. Dar, F. T. Eickemeyer, N. Arora, Q. Hu, J. Luo, Y. Liu, S. M. Zakeeruddin, A. Hagfeldt, J. Arbiol, W. Huang, Q. Gong, T. P. Russell, R. H. Friend, M. Grätzel, and R. Zhu, Enabling full-scale grain boundary mitigation in polycrystalline perovskite solids, *Sci. Adv.* 8(35), eabo3733 (2022)
33. J. Wang, J. Li, Q. Tan, L. Li, J. Zhang, J. Zang, P. Tan, J. Zhang, and D. Li, Controllable synthesis of two-dimensional Ruddlesden–Popper-type perovskite heterostructures, *J. Phys. Chem. Lett.* 8(24), 6211 (2017)
34. A. Dey, A. F. Richter, T. Debnath, H. Huang, L. Polavarapu, and J. Feldmann, Transfer of direct to indirect bound excitons by electron intervalley scattering in $Cs_2AgBiBr_6$ double perovskite nanocrystals, *ACS Nano* 14(5), 5855 (2020)
35. S. K. Rajendran, M. Wei, H. Ohadi, A. Ruseckas, G. A. Turnbull, and I. D. W. Samuel, Low threshold polariton lasing from a solution-processed organic semiconductor in a planar microcavity, *Adv. Opt. Mater.* 7(12), 1801791 (2019)
36. S. Guo, Y. Li, Y. Mao, W. Tao, K. Bu, T. Fu, C. Zhao, H. Luo, Q. Hu, H. Zhu, E. Shi, W. Yang, L. Dou, and X. Lü, Reconfiguring band-edge states and charge distribution of organic semiconductor-incorporated 2D perovskites via pressure gating, *Sci. Adv.* 8(44), eadd1984 (2022)
37. N. Zhou and H. Zhou, Spacer organic cation engineering for quasi-2D metal halide perovskites and the optoelectronic application, *Small Struct.* 3(7), 2100232 (2022)
38. Z. Wang, Q. Wei, X. Liu, L. Liu, X. Tang, J. Guo, S. Ren, G. Xing, D. Zhao, and Y. Zheng, Spacer cation tuning enables vertically oriented and graded quasi-2D perovskites for efficient solar cells, *Adv. Funct. Mater.* 31(5), 2008404 (2021)
39. Y. Jiang, M. Cui, S. Li, C. Sun, Y. Huang, J. Wei, L. Zhang, M. Lv, C. Qin, Y. Liu, and M. Yuan, Reducing the impact of Auger recombination in quasi-2D perovskite light-emitting diodes, *Nat. Commun.* 12(1), 336 (2021)
40. R. Wang, X. Dong, Q. Ling, Q. Fu, Z. Hu, Z. Xu, H. Zhang, Q. Li, and Y. Liu, Spacer engineering for 2D Ruddlesden–Popper perovskites with an ultralong carrier lifetime of over 18 μs enable efficient solar cells, *ACS Energy Lett.* 7(10), 3656 (2022)
41. T. Umebayashi, K. Asai, T. Kondo, and A. Nakao, Electronic structures of lead iodide based low-dimensional crystals, *Phys. Rev. B* 67(15), 155405 (2003)
42. Y. Fu, H. Zhu, J. Chen, M. P. Hautzinger, X. Y. Zhu, and S. Jin, Metal halide perovskite nanostructures for optoelectronic applications and the study of physical properties, *Nat. Rev. Mater.* 4(3), 169 (2019)
43. J. Li, J. Ma, X. Cheng, Z. Liu, Y. Chen, and D. Li, Anisotropy of excitons in two-dimensional perovskite crystals, *ACS Nano* 14(2), 2156 (2020)
44. Y. Zhang, M. Sun, N. Zhou, B. Huang, and H. Zhou, Electronic tunability and mobility anisotropy of quasi-2D perovskite single crystals with varied spacer cations, *J. Phys. Chem. Lett.* 11(18), 7610 (2020)
45. M. Wang, H. Zou, J. Zhang, T. Wu, H. Xu, S. Haacke, and B. Hu, Extremely long spin lifetime of light-emitting states in quasi-2D perovskites through orbit–orbit interaction, *J. Phys. Chem. Lett.* 11(9), 3647 (2020)
46. H. Li, X. Zhang, H. Wang, J. Yu, K. Li, Z. Wei, D. Li, and R. Chen, Optical characteristics of self-trapped excitons in 2D $(iso\text{-}BA)_2PbI_4$ perovskite crystals, *Photon. Res.* 10(2), 594 (2022)
47. J. Li, H. Wang, and D. Li, Self-trapped excitons in two-dimensional perovskites, *Front. Optoelectron.* 13(3), 225 (2020)
48. J. C. Blancon, H. Tsai, W. Nie, C. C. Stoumpos, L. Pedesseau, C. Katan, M. Kepenekian, C. M. M. Soe, K. Appavoo, M. Y. Sfeir, S. Tretiak, P. M. Ajayan, M. G. Kanatzidis, J. Even, J. J. Crochet, and A. D. Mohite, Extremely efficient internal exciton dissociation through edge states in layered 2D perovskites, *Science* 355(6331), 1288 (2017)
49. Z. Liu, M. Hu, J. Du, T. Shi, Z. Wang, Z. Zhang, Z. Hu, Z. Zhan, K. Chen, W. Liu, J. Tang, H. Zhang, Y. Leng, and R. Li, Subwavelength-polarized quasi-two-dimensional perovskite single-mode nanolaser, *ACS Nano* 15(4), 6900 (2021)
50. D. Ye, Z. Li, W. Chen, K. O. Ighodalo, P. Xiao, T. Chen, and Z. Xiao, Stable yellow light-emitting diodes based on quasi-two-dimensional perovskites, *ACS Appl. Mater. Interfaces* 14(30), 34918 (2022)
51. Y. Yang, S. Xu, Z. Ni, C. H. Van Brackle, L. Zhao, X. Xiao, X. Dai, and J. Huang, Highly efficient pure-blue light-emitting diodes based on rubidium and chlorine alloyed metal halide perovskite, *Adv. Mater.* 33(33), 2100783 (2021)
52. C. H. A. Li, P. Geng, S. B. Shivarudraiah, M. Ng, X. F. Zhang, B. Xu, L. Guo, and J. E. Halpert, The multiple roles of metal ion dopants in spectrally stable, efficient quasi-2D perovskite sky-blue light-emitting devices, *Adv. Opt. Mater.* 9(21), 2100860 (2021)
53. L. Yang, Y. Zhang, J. Ma, P. Chen, Y. Yu, and M. Shao, Pure red light-emitting diodes based on quantum confined quasi-two-dimensional perovskites with cospacer cations, *ACS Energy Lett.* 6(7), 2386 (2021)
54. P. Liu, W. Cai, C. Zhao, S. Zhang, P. Nie, W. Xu, H. Meng, H. Fu, and G. Wei, Quasi-2D $CsPbBr_xI_{3-x}$ composite thin films for efficient and stable red perovskite light-emitting diodes, *Adv. Opt. Mater.* 9(24), 2101419 (2021)
55. M. Worku, A. Ben-Akacha, S. Sridhar, J. R. Frick, S. Yin, Q. He, A. J. Robb, M. Chaaban, H. Liu, J. S. R. V. Winfred, K. Hanson, F. So, D. Dougherty, and B. Ma, Band edge control of quasi-2D metal halide perovskites for blue light-emitting diodes with enhanced performance, *Adv. Funct. Mater.* 31(45), 2103299 (2021)
56. S. Liu, Z. Guo, X. Wu, X. Liu, Z. Huang, L. Li, J. Zhang, H. Zhou, L. D. Sun, and C. H. Yan, Zwitterions narrow distribution of perovskite quantum wells for blue light-emitting diodes with efficiency exceeding 15%, *Adv. Mater.* 35(3), 2208078 (2023)

57. X. Zhang, X. Wang, H. Liu, and R. Chen, Defect engineering of metal halide perovskite optoelectronic devices, *Prog. Quantum Electron.* 86, 100438 (2022)
58. R. Li, B. Li, X. Fang, D. Wang, Y. Shi, X. Liu, R. Chen, and Z. Wei, Self-structural healing of encapsulated perovskite microcrystals for improved optical and thermal stability, *Adv. Mater.* 33(21), 2100466 (2021)
59. Z. Ren, L. Li, J. Yu, R. Ma, X. Xiao, R. Chen, K. Wang, X. W. Sun, W. J. Yin, and W. C. H. Choy, Simultaneous low-order phase suppression and defect passivation for efficient and stable blue light-emitting diodes, *ACS Energy Lett.* 5(8), 2569 (2020)
60. T. Cheng, C. Qin, S. Watanabe, T. Matsushima, and C. Adachi, Stoichiometry control for the tuning of grain passivation and domain distribution in green quasi-2D metal halide perovskite films and light-emitting diodes, *Adv. Funct. Mater.* 30(24), 2001816 (2020)
61. Y. Gao, Y. Liu, F. Zhang, X. Bao, Z. Xu, X. Bai, M. Lu, Y. Wu, Z. Wu, Y. Zhang, Q. Wang, X. Gao, Y. Wang, Z. Shi, J. Hu, W. W. Yu, and Y. Zhang, High-performance perovskite light-emitting diodes enabled by passivating defect and constructing dual energy-transfer pathway through functional perovskite nanocrystals, *Adv. Mater.* 34(43), 2207445 (2022)
62. D. Zhang, Y. Fu, H. Zhan, C. Zhao, X. Gao, C. Qin, and L. Wang, Suppressing thermal quenching via defect passivation for efficient quasi-2D perovskite light-emitting diodes, *Light Sci. Appl.* 11(1), 69 (2022)
63. D. Zhang, Y. Fu, W. Wu, B. Li, H. Zhu, H. Zhan, Y. Cheng, C. Qin, and L. Wang, Comprehensive passivation for high-performance quasi-2D perovskite LEDs, *Small* 19(11), 2206927 (2023)
64. X. Bao, Y. Gao, Y. Liu, Z. Xu, F. Zhang, M. Lu, Z. Wu, Y. Wu, Q. Wang, Y. Zhang, Y. Wang, Z. Shi, J. Hu, and X. Bai, Molecular bridging strategy enables high performance and stable quasi-2D perovskite light-emitting devices, *ACS Energy Lett.* 8(2), 1018 (2023)
65. T. Liu, Z. Zhang, Q. Wei, B. Wang, K. Wang, J. Guo, C. Liang, D. Zhao, S. Chen, Y. Tang, Y. Zhou, and G. Xing, Tailoring quasi-2D perovskite thin films via nanocrystals mediation for enhanced electroluminescence, *Chem. Eng. J.* 411, 128511 (2021)
66. M. Cinquino, A. Fieramosca, R. Mastria, L. Polimeno, A. Moliterni, V. Olieric, N. Matsugaki, R. Panico, M. De Giorgi, G. Gigli, C. Giannini, A. Rizzo, D. Sanvitto, and L. De Marco, Managing growth and dimensionality of quasi 2D perovskite single-crystalline flakes for tunable excitons orientation, *Adv. Mater.* 33(48), 2102326 (2021)
67. C. Lin, K. Niu, Y. Qi, Y. Liu, X. Zhu, S. He, Z. Zhou, Y. Jin, H. He, and Z. Ye, Dimension tailoring via anti-solvent enables efficient perovskite light-emitting diodes, *Mater. Today Nano* 17, 100170 (2022)
68. Y. Nah, D. Solanki, Y. Dong, J. A. Röhr, A. D. Taylor, S. Hu, E. H. Sargent, and D. H. Kim, Narrowing the phase distribution of quasi-2D perovskites for stable deep-blue electroluminescence, *Adv. Sci. (Weinh.)* 9(24), 2201807 (2022)
69. J. Zhang, X. Zhu, M. Wang, and B. Hu, Establishing charge-transfer excitons in 2D perovskite heterostructures, *Nat. Commun.* 11(1), 2618 (2020)
70. E. Shi, B. Yuan, S. B. Shiring, Y. Gao, Y. Akriti, Y. Guo, C. Su, M. Lai, P. Yang, J. Kong, B. M. Savoie, Y. Yu, and L. Dou, Two-dimensional halide perovskite lateral epitaxial heterostructures, *Nature* 580(7805), 614 (2020)
71. M. Li, Q. Gao, P. Liu, Q. Liao, H. Zhang, J. Yao, W. Hu, Y. Wu, and H. Fu, Amplified spontaneous emission based on 2D Ruddlesden–Popper perovskites, *Adv. Funct. Mater.* 28(17), 1707006 (2018)
72. G. Ding, X. He, H. Zhang, and H. Fu, Ethanol-assisted synthesis of two-dimensional TiN(ii) halide perovskite single crystals for amplified spontaneous emission, *J. Mater. Chem. C* 10(30), 10902 (2022)
73. Q. Shang, Y. Wang, Y. Zhong, Y. Mi, L. Qin, Y. Zhao, X. Qiu, X. Liu, and Q. Zhang, Unveiling structurally engineered carrier dynamics in hybrid quasi-two-dimensional perovskite thin films toward controllable emission, *J. Phys. Chem. Lett.* 8(18), 4431 (2017)
74. Y. Liang, Q. Shang, M. Li, S. Zhang, X. Liu, and Q. Zhang, Solvent recrystallization-enabled green amplified spontaneous emissions with an ultra-low threshold from pinhole-free perovskite films, *Adv. Funct. Mater.* 31(48), 2106108 (2021)
75. C. Qin, S. Zhang, Z. Zhou, T. Han, J. Song, S. Ma, G. Jia, Z. Jiao, Z. Zhu, X. Chen, and Y. Jiang, Low amplified spontaneous emission threshold from 2-thiophenemethylammonium quasi-2D perovskites via phase engineering, *Opt. Express* 30(20), 36541 (2022)
76. Y. Shi, R. Li, G. Yin, X. Zhang, X. Yu, B. Meng, Z. Wei, and R. Chen, Laser-induced secondary crystallization of $CsPbBr_3$ perovskite film for robust and low threshold amplified spontaneous emission, *Adv. Funct. Mater.* 32(49), 2207206 (2022)
77. G. Li, K. Lin, K. Zhao, Y. Huang, T. Ji, L. Shi, Y. Hao, Q. Xiong, K. Zheng, T. Pullerits, and Y. Cui, Localized bound multiexcitons in engineered quasi-2D perovskites grains at room temperature for efficient lasers, *Adv. Mater.* 35(20), 2211591 (2023)
78. Y. Yang, X. Peng, C. Qin, Y. Lian, J. Gao, and X. Yang, Accelerating energy funnel and charge transport of quasi-2D perovskites for efficient sky blue and white-light-emitting devices, *ACS Photonics* 9(1), 163 (2022)
79. I. Allegro, Y. Li, B. S. Richards, U. W. Paetzold, U. Lemmer, and I. A. Howard, Bimolecular and Auger recombination in phase-stable perovskite thin films from cryogenic to room temperature and their effect on the amplified spontaneous emission threshold, *J. Phys. Chem. Lett.* 12(9), 2293 (2021)
80. S. Huang, N. Liu, Z. Liu, Z. Zhan, Z. Hu, Z. Du, Z. Zhang, J. Luo, J. Du, J. Tang, and Y. Leng, Enhanced amplified spontaneous emission in quasi-2D perovskite by facilitating energy transfer, *ACS Appl. Mater. Interfaces* 14(29), 33842 (2022)
81. J. Li, L. Zhang, Z. Chu, C. Dong, J. Jiang, Z. Yin, J. You, J. Wu, W. Lan, and X. Zhang, Amplified spontaneous emission with a low threshold from quasi-2D perovskite films via phase engineering and surface passivation, *Adv. Opt. Mater.* 10(6), 2102563 (2022)
82. M. Cui, C. Qin, Y. Jiang, M. Yuan, L. Xu, D. Song, Y. Jiang, and Y. Liu, Direct observation of competition between amplified spontaneous emission and Auger

recombination in quasi-two-dimensional perovskites, *J. Phys. Chem. Lett.* 11(14), 5734 (2020)
83. Y. Li, I. Allegro, M. Kaiser, A. J. Malla, B. S. Richards, U. Lemmer, U. W. Paetzold, and I. A. Howard, Exciton versus free carrier emission: implications for photoluminescence efficiency and amplified spontaneous emission thresholds in quasi-2D and 3D perovskites, *Mater. Today* 49, 35 (2021)
84. M. Li, Q. Shang, C. Li, S. Li, Y. Liang, W. Yu, C. Wu, L. Zhao, Y. Zhong, W. Du, X. Wu, Z. Jia, Y. Gao, H. Chen, X. Liu, S. Guo, Q. Liao, G. Xing, L. Xiao, and Q. Zhang, High optical gain of solution-processed mixed-cation $CsPbBr_3$ thin films towards enhanced amplified spontaneous emission, *Adv. Funct. Mater.* 31(25), 2102210 (2021)
85. X. He, H. Gong, H. Huang, Y. Li, J. Ren, Y. Li, Q. Liao, T. Gao, and H. Fu, Multicolor biexciton lasers based on 2D perovskite single crystalline flakes, *Adv. Opt. Mater.* 10(15), 2200238 (2022)
86. Z. Chu, T. Guo, S. Zhao, H. Chen, Y. Li, W. Xu, and G. Ran, Quasi 2D perovskite single-mode vertical-cavity lasers through large-area film transfer, *Appl. Phys. Lett.* 120(12), 121104 (2022)
87. C. Qin, A. S. D. Sandanayaka, C. Zhao, T. Matsushima, D. Zhang, T. Fujihara, and C. Adachi, Stable room-temperature continuous-wave lasing in quasi-2D perovskite films, *Nature* 585(7823), 53 (2020)
88. L. Lei, D. Seyitliyev, S. Stuard, J. Mendes, Q. Dong, X. Fu, Y. A. Chen, S. He, X. Yi, L. Zhu, C. H. Chang, H. Ade, K. Gundogdu, and F. So, Efficient energy funneling in quasi-2D perovskites: From light emission to lasing, *Adv. Mater.* 32(16), 1906571 (2020)
89. G. Liu, S. Jia, J. Wang, Y. Li, H. Yang, S. Wang, and Q. Gong, Toward microlasers with artificial structure based on single-crystal ultrathin perovskite films, *Nano Lett.* 21(20), 8650 (2021)
90. Y. Liang, Q. Shang, Q. Wei, L. Zhao, Z. Liu, J. Shi, Y. Zhong, J. Chen, Y. Gao, M. Li, X. Liu, G. Xing, and Q. Zhang, Lasing from mechanically exfoliated 2D homologous Ruddlesden–Popper perovskite engineered by inorganic layer thickness, *Adv. Mater.* 31(39), 1903030 (2019)
91. W. Gao, Q. Wei, T. Wang, J. Xu, L. Zhuang, M. Li, K. Yao, and S. F. Yu, Two-photon lasing from two-dimensional homologous Ruddlesden–Popper perovskite with giant nonlinear absorption and natural microcavities, *ACS Nano* 16(8), 13082 (2022)
92. H. Dong, C. Zhang, X. Liu, J. Yao, and Y. S. Zhao, Materials chemistry and engineering in metal halide perovskite lasers, *Chem. Soc. Rev.* 49(3), 951 (2020)
93. C. Fruhling, K. Wang, S. Chowdhury, X. Xu, J. Simon, A. Kildishev, L. Dou, X. Meng, A. Boltasseva, and V. M. Shalaev, Coherent random lasing in subwavelength quasi-2D perovskites, *Laser Photonics Rev.* 17(4), 2200314 (2023)
94. P. K. Roy, R. K. Ulaganathan, C. M. Raghavan, S. M. Mhatre, H. I. Lin, W. L. Chen, Y. M. Chang, A. Rozhin, Y. T. Hsu, Y. F. Chen, R. Sankar, F. C. Chou, and C. T. Liang, Unprecedented random lasing in 2D organolead halide single-crystalline perovskite microrods, *Nanoscale* 12(35), 18269 (2020)
95. T. Y. Liu, H. Wang, M. S. Song, L. Y. Zhao, Z. F. Hu, and H. Y. Wang, Dynamics of spin-dependent polariton–polariton interactions in two-dimensional layered halide organic perovskite microcavities, *Laser Photonics Rev.* 16(10), 2200176 (2022)
96. A. Fieramosca, L. Polimeno, V. Ardizzone, L. De Marco, M. Pugliese, V. Maiorano, M. De Giorgi, L. Dominici, G. Gigli, D. Gerace, D. Ballarini, and D. Sanvitto, Two-dimensional hybrid perovskites sustaining strong polariton interactions at room temperature, *Sci. Adv.* 5(5), eaav9967 (2019)
97. J. Wang, R. Su, J. Xing, D. Bao, C. Diederichs, S. Liu, T. C. H. Liew, Z. Chen, and Q. Xiong, Room temperature coherently coupled exciton–polaritons in two-dimensional organic–inorganic perovskite, *ACS Nano* 12(8), 8382 (2018)
98. S. B. Anantharaman, C. E. Stevens, J. Lynch, B. Song, J. Hou, H. Zhang, K. Jo, P. Kumar, J. C. Blancon, A. D. Mohite, J. R. Hendrickson, and D. Jariwala, Self-hybridized polaritonic emission from layered perovskites, *Nano Lett.* 21(14), 6245 (2021)
99. L. Polimeno, G. Lerario, M. De Giorgi, L. De Marco, L. Dominici, F. Todisco, A. Coriolano, V. Ardizzone, M. Pugliese, C. T. Prontera, V. Maiorano, A. Moliterni, C. Giannini, V. Olieric, G. Gigli, D. Ballarini, Q. Xiong, A. Fieramosca, D. D. Solnyshkov, G. Malpuech, and D. Sanvitto, Tuning of the Berry curvature in 2D perovskite polaritons, *Nat. Nanotechnol.* 16(12), 1349 (2021)
100. K. Łempicka-Mirek, M. Król, H. Sigurdsson, A. Wincukiewicz, P. Morawiak, R. Mazur, M. Muszyński, W. Piecek, P. Kula, T. Stefaniuk, M. Kamińska, L. De Marco, P. G. Lagoudakis, D. Ballarini, D. Sanvitto, J. Szczytko, and B. Piętka, Electrically tunable Berry curvature and strong light–matter coupling in liquid crystal microcavities with 2D perovskite, *Sci. Adv.* 8(40), eabq7533 (2022)
101. J. E. Park, R. López-Arteaga, A. D. Sample, C. R. Cherqui, I. Spanopoulos, J. Guan, M. G. Kanatzidis, G. C. Schatz, E. A. Weiss, and T. W. Odom, Polariton dynamics in two-dimensional Ruddlesden–Popper perovskites strongly coupled with plasmonic lattices, *ACS Nano* 16(3), 3917 (2022)
102. N. H. M. Dang, D. Gerace, E. Drouard, G. Trippé-Allard, F. Lédée, R. Mazurczyk, E. Deleporte, C. Seassal, and H. S. Nguyen, Tailoring dispersion of room-temperature exciton–polaritons with perovskite-based subwavelength metasurfaces, *Nano Lett.* 20(3), 2113 (2020)
103. S. Kim, B. H. Woo, S. C. An, Y. Lim, I. C. Seo, D. S. Kim, S. Yoo, Q. H. Park, and Y. C. Jun, Topological control of 2D perovskite emission in the strong coupling regime, *Nano Lett.* 21(23), 10076 (2021)
104. R. Su, C. Diederichs, J. Wang, T. C. H. Liew, J. Zhao, S. Liu, W. Xu, Z. Chen, and Q. Xiong, Room-temperature polariton lasing in all-inorganic perovskite nanoplatelets, *Nano Lett.* 17(6), 3982 (2017)
105. L. Polimeno, A. Fieramosca, G. Lerario, M. Cinquino, M. De Giorgi, D. Ballarini, F. Todisco, L. Dominici, V. Ardizzone, M. Pugliese, C. T. Prontera, V. Maiorano, G. Gigli, L. De Marco, and D. Sanvitto, Observation of two thresholds leading to polariton condensation in

2D hybrid perovskites, *Adv. Opt. Mater.* 8(16), 2000176 (2020)

106. X. Yang, X. Zhang, J. Deng, Z. Chu, Q. Jiang, J. Meng, P. Wang, L. Zhang, Z. Yin, and J. You, Efficient green light-emitting diodes based on quasi-two-dimensional composition and phase engineered perovskite with surface passivation, *Nat. Commun.* 9(1), 570 (2018)
107. N. Zhou, Y. Shen, L. Li, S. Tan, N. Liu, G. Zheng, Q. Chen, and H. Zhou, The exploration of crystallization kinetics in quasi two-dimensional perovskite and high performance solar cells, *J. Am. Chem. Soc.* 140(1), 459 (2018)
108. T. L. Leung, I. Ahmad, A. A. Syed, A. M. C. Ng, J. Popović, and A. B. Djurišić, Stability of 2D and quasi-2D perovskite materials and devices, *Commun. Mater.* 3(1), 63 (2022)
109. C. Wang, G. Dai, J. Wang, M. Cui, Y. Yang, S. Yang, C. Qin, S. Chang, K. Wu, Y. Liu, and H. Zhong, Low-threshold blue quasi-2D perovskite laser through domain distribution control, *Nano Lett.* 22(3), 1338 (2022)
110. Y. Yang, F. Gao, S. Gao, and S. H. Wei, Origin of the stability of two-dimensional perovskites: A first-principles study, *J. Mater. Chem. A* 6(30), 14949 (2018)
111. J. Wang, D. Li, L. Mu, M. Li, Y. Luo, B. Zhang, C. Mai, B. Guo, L. Lan, J. Wang, H. L. Yip, and J. Peng, Inkjet-printed full-color matrix quasi-two-dimensional perovskite light-emitting diodes, *ACS Appl. Mater. Interfaces* 13(35), 41773 (2021)
112. F. Chen, H. Li, H. Zhou, S. Luo, Z. Sun, Z. Ye, F. Sun, J. Wang, Y. Zheng, X. Chen, H. Xu, H. Xu, T. Byrnes, Z. Chen, and J. Wu, Optically controlled femtosecond polariton switch at room temperature, *Phys. Rev. Lett.* 129(5), 057402 (2022)
113. N. G. Berloff, M. Silva, K. Kalinin, A. Askitopoulos, J. D. Töpfer, P. Cilibrizzi, W. Langbein, and P. G. Lagoudakis, Realizing the classical XY Hamiltonian in polariton simulators, *Nat. Mater.* 16(11), 1120 (2017)
114. Y. Wang, M. Zhi, Y. Q. Chang, J. P. Zhang, and Y. Chan, Stable, ultralow threshold amplified spontaneous emission from $CsPbBr_3$ nanoparticles exhibiting trion gain, *Nano Lett.* 18(8), 4976 (2018)
115. Q. Shang, M. Li, L. Zhao, D. Chen, S. Zhang, S. Chen, P. Gao, C. Shen, J. Xing, G. Xing, B. Shen, X. Liu, and Q. Zhang, Role of the exciton–polariton in a continuous-wave optically pumped $CsPbBr_3$ perovskite laser, *Nano Lett.* 20(9), 6636 (2020)
116. J. Song, Q. Shang, X. Deng, Y. Liang, C. Li, X. Liu, Q. Xiong, and Q. Zhang, Continuous-wave pumped perovskite lasers with device area below 1 μm^2, *Adv. Mater.* 35(30), 2302170 (2023)
117. Z. Ren, J. Yu, Z. Qin, J. Wang, J. Sun, C. C. S. Chan, S. Ding, K. Wang, R. Chen, K. S. Wong, X. Lu, W. J. Yin, and W. C. H. Choy, High-performance blue perovskite light-emitting diodes enabled by efficient energy transfer between coupled quasi-2D perovskite layers, *Adv. Mater.* 33(1), 2005570 (2021)
118. Z. Ren, J. Sun, J. Yu, X. Xiao, Z. Wang, R. Zhang, K. Wang, R. Chen, Y. Chen, and W. C. H. Choy, High-performance blue quasi-2D perovskite light-emitting diodes via balanced carrier confinement and transfer, *Nano-Micro Lett.* 14(1), 66 (2022)